Physica D 347 (2017) 90–108

Contents lists available at ScienceDirect

Physica D

journal homepage: www.elsevier.com/locate/physd

Full analysis of small hypercycles with short-circuits in prebiotic evolution

Josep Sardanyés [a,b,*], J. Tomás Lázaro [c,d], Antoni Guillamon [d,e], Ernest Fontich [d,f]

[a] ICREA-Complex Systems Lab, Department of Experimental and Health Sciences, Universitat Pompeu Fabra, Dr. Aiguader 88, 08003 Barcelona, Spain
[b] Institut de Biologia Evolutiva, CSIC-Universitat Pompeu Fabra, Passeig Marítim de la Barceloneta 37, 08003 Barcelona, Spain
[c] Departament de Matemàtiques, Universitat Politècnica de Catalunya, Av. Diagonal 647, 08028 Barcelona, Spain
[d] Barcelona Graduate School of Mathematics BGSMath, Spain
[e] Departament de Matemàtiques, Universitat Politècnica de Catalunya, Av. Gregorio Marañón 44-50, 08028 Barcelona, Spain
[f] Departament de Matemàtiques i Informàtica, Universitat de Barcelona, Gran Via de les Corts Catalanes 585, 08007 Barcelona, Spain

HIGHLIGHTS

- We study the population dynamics of small hypercycles with short-circuits.
- Mean field and cellular automata models are used to study the dynamics and bifurcations.
- We identify a rich repertoire of transcritical and saddle–node bifurcations.
- Small hypercycles are shown to be vulnerable to catalytic short-circuits.
- The vulnerability increases at growing degradation rates of the hypercycle members.

ARTICLE INFO

Article history:
Received 31 May 2016
Accepted 19 December 2016
Available online 5 January 2017
Communicated by S. Coombes

Keywords:
Bifurcations
Cooperation
Nonlinear dynamics
Origins of Life
Short-circuits
Hypercycles

ABSTRACT

It is known that hypercycles are sensitive to the so-called parasites and short-circuits. While the impact of parasites has been widely investigated for well-mixed and spatial hypercycles, the effect of short-circuits in hypercycles remains poorly understood. In this article we analyze the mean field and spatial dynamics of two small, asymmetric hypercycles with short-circuits. Specifically, we analyze a two-member hypercycle where one of the species contains an auto-catalytic loop, as the simplest hypercycle with a short-circuit. Then, we extend this system by adding another species that closes a three-member hypercycle while keeping the auto-catalytic short-circuit and the two-member cycle. The mean field model allows us to discard the presence of stable or unstable periodic orbits for both systems. We characterize the bifurcations and transitions involved in the dominance of the short-circuits i.e., in the reduction of the hypercycles' size. The spatial simulations reveal a random-like and mixed distribution of the replicators in the all-species coexistence, ruling out the presence of large-scale spatial patterns such as spirals or spots typical of larger, oscillating hypercycles. A Monte Carlo sampling of the parameter space for the well-mixed and the spatial models reveals that the probability of finding stable hypercycles with short-circuits drastically diminishes from the two-member to the three-member system, especially at growing degradation rates of the replicators. These findings pose a big constraint in the increase of hypercycle's size and complexity under the presence of inner cycles, suggesting the importance of a rapid growth of hypercycles able to generate spatial structures (e.g., rotating spirals) prior to the emergence of inner cycles. Our results can also be useful for the future design and implementation of synthetic cooperative systems containing catalytic short-circuits.

1. Introduction

The precise description and prediction of the steps preceding the origin of life in our planet is one of the most challenging and hard problems in science. Despite this difficulty, several theories

* Corresponding author at: ICREA-Complex Systems Lab, Department of Experimental and Health Sciences, Universitat Pompeu Fabra, Dr. Aiguader 88, 08003 Barcelona, Spain.
E-mail address: josep.sardanes@upf.edu (J. Sardanyés).

http://dx.doi.org/10.1016/j.physd.2016.12.004
0167-2789/

have been suggested in the last decades to describe possible scenarios behind the emergence of the first stable replicating systems, in what has been labeled as the crystallization of life in the framework of phase transitions phenomena [1]. The first groundbreaking discovery by Miller and Urey, which proved the Oparin and Haldane hypothesis, revealed that organic molecules (mainly two types of amino acids) could be synthesized from inorganic ones in the Earth primitive conditions [2]. Miller's approach opened a new era and since then, geological, physical, and chemical requirements for the beginning of life have been discussed with diligence [3–6]. For instance, the possibility of abiotic synthesis of the building blocks of RNA and DNA [7–9]. Subsequent research on the understanding of the origin of life was deepened substantially by the theory of Eigen and Schuster [10], who put evolution and heredity into the picture using biochemical and more formal mathematical arguments. They argued that at spontaneous error rates during replication of about 10^{-2} changes per nucleotide [11], the first faithfully reproducing molecules should be single-stranded RNAs not exceeding 50–100 nucleotides [10,12]. This conjecture arose within the theoretical framework of quasispecies theory [13]. Quasispecies theory was conceived as a chemically-plausible mathematical formulation for the dynamics and evolution of information of macromolecules under large mutation rates (as expected in prebiotic evolution). Roughly, a quasispecies is a set of sequences that is generated by replication–mutation dynamics of an initial template (often named the master sequence). Differently to the concept of species, a quasispecies is a set of closely-related mutants which are (as a whole, and not individually) under the filter of natural selection.

Assuming RNAs as the building blocks of the first living forms, stability against hydrolysis [14] and replicability [15] might favor RNAs that display a loop and stem structure similar to that of modern tRNAs [12], which are about 76–90 nucleotides long. Indeed, some smaller, functional ribozymes (i.e., RNA with catalytic activity) of about 50 nucleotides have been described in viroids [16] and other RNAs [17]. Some of these hypothetic prebiotic RNAs were supposed to participate in ribosome-free translation of an appropriate messenger as suggested in [18]. In this sense, ligase reactions by RNA catalysts are known to occur even with small RNA sequences [19]. The RNA-first theory has some powerful arguments in its favor [1]. First of all, all life is based on RNA/DNA as the stable storage of genetic information. Second, RNA can act as informational carrier and enzyme at the same time, thus encoding in the same molecule the two characteristics needed for evolutionary potential: message and reproduction. Third, RNA is a beautiful example of Schrödinger's aperiodic crystals, which are point–point local templating complements [1]. Also, it is known that certain introns can catalyze their own excision from single-stranded RNA (ssRNA). Furthermore, the same RNA sequences can catalyze transesterification reactions for elongation of one monomer [20], ligation of two independent ssRNAs [21,22], and cleavage of RNA into smaller sequences [20,16]. Despite the previous ribozyme reactions, self-replication through RNA-catalyzed templated RNA synthesis seems to be quite limited. However, recent *in vitro* experiments evolving catalysts at sub-zero temperatures revealed that the combination of RNAs with cold-adaptative mutations with a previously described 5′ extension operating at ambient temperatures enabled catalyzing the synthesis of an RNA sequence longer than itself (adding up to 206 nucleotides) [23]. Furthermore, a recent work by Vaidya and colleagues revealed that mixtures of RNA fragments that self-assemble into ribozymes spontaneously formed cooperative catalytic cycles, providing experimental evidences for the viability of spontaneous hypercycles (see below for the definition of hypercycles) formation from existing RNAs [24].

The understanding of the properties of the first replicating molecules is crucial to disentangle the origin of life problem. Such replicating entities could carry compositional [25–27] or genetically-encoded [13,10] information. A simple and thus plausible initial scenario concerning genetically-encoded systems could be given by a set of ribozymes replicating at extremely large error rates due to the lack of proof reading mechanisms. Such a system, similar to a quasi-species, could perform a wide and rapid exploration of the sequence space thus being able to find genotypes with catalytic phenotypes capable of forming the so-called hypercycles. Hypercycles are sets of macromolecules that are able to catalyze the reproduction of other macromolecules [10] (see also Ref. [28]). With auto-catalysis, a given replicator type catalyzes its own replication, while when a given replicator type catalyzes the replication of a different macromolecule then the relation is called hetero-catalytic (or cross-catalytic). Usually, the term hypercycle is used for sets of molecules with a cyclic and closed catalytic architecture, where the catalytic interactions from one member to the other (or to itself) are named catalytic connections or links (using the networks jargon). These hypercycles could contain several catalytically-connected molecules able to increase the information of the entire system while keeping the individual replicators below the critical length imposed by the error threshold [13,29]. Since no molecule in the hypercycle can outcompete another because they are forced to cooperate, a large genetic message given by all the information of all templates could be attained, thus crossing the information threshold [13].

Following the previous scenario, it seems reasonable to envision the origin of life as a process starting from a small set of RNA molecules with hypercyclic organization. Such small sets could also become the nucleating agents towards more complex and disordered catalytic networks able to unleash the major transition towards more diverse, fully functional, self-replicating systems, as suggested by Kauffman [1,30] (see also [31,32]), beyond the cyclic architecture proposed by Eigen and Schuster. Such proto-genetic structures could have then grown in size and evolved towards more complex structures by means of spatial organization [33–35] or compartmentalization in protocells [12].

Hypercycles, however, due to the nature of their interactions, were criticized as stable systems involved in the origin of life since they are sensitive to the so-called parasites and short-circuits [10,36]. Parasites are replicators that receive catalysis from another species but do not reciprocate the catalytic aid [10]. Short-circuits, which can be of different nature, are catalytic connections generating inner and smaller catalytic sub-cycles [13,27]. Short-circuits have been suggested to pose a serious problem towards the growth of hypercycle systems, since smallest and thus fastest catalytic cycles may outcompete the larger and slower ones, thus constraining hypercycles' size, complexity, and functionality. Despite this intuitive assertion, few literature has addressed the impact of short-circuits in hypercycles (see below). Oppositely, multitude of articles have analyzed the impact of parasites, showing that they can resist parasites by means of spatial self-structuring [33,35,34].

The effect of different configurations and sub-cycles in spatial hypercycles was addressed numerically in [35]. This approach revealed that hypercycles are able to coexist with inner cycles in an exclusive manner by means of spiral patterns [35]. According to [35], spatial self-structuring seems to play an important role in the stability of hypercycles with short-circuits, although independent communities are formed and thus there exists a physical separation between the sets of cycles forming the entire system. Actually, the simulations in [35] revealed that asymmetries in diffusion constants could involve the outcompetition of different cycles. Similarly, changes in the kinetic constants also involved processes of outcompetition between cycles, resulting in the loss of some of the hypercycle members (involving a loss of information).

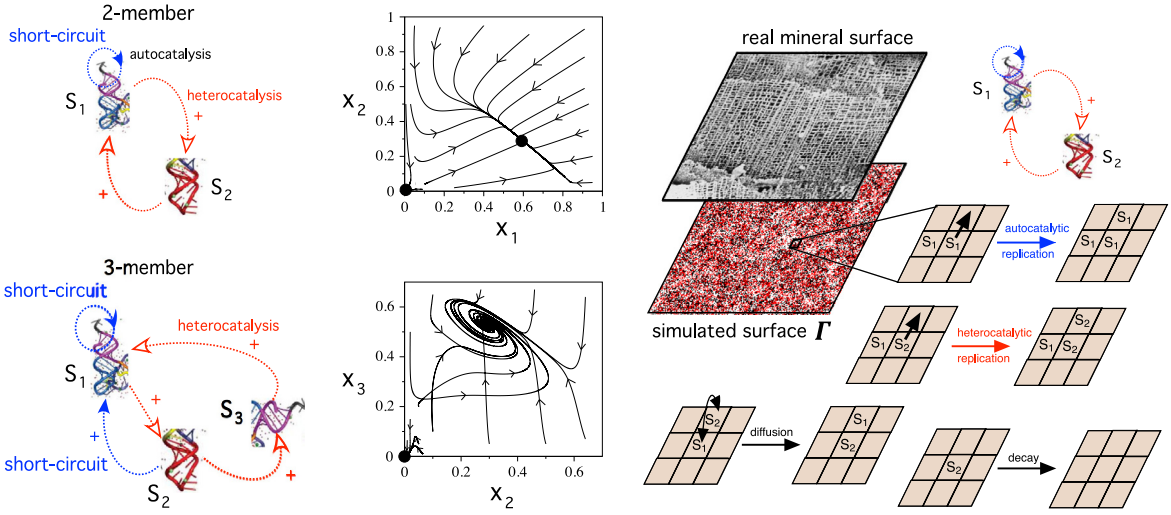

(a) Hypercycles. (b) Mean field dynamics. (c) Spatial dynamics.

Fig. 1. (a) Minimal hypercycles with short-circuits: (up) two-member hypercycle (S_1 and S_2) with an auto-catalytic short-circuit (S_1); (down) three-member hypercycle (S_1, S_2, and S_3) including the two-member hypercycle and the auto-catalytic replicator. (b) Dynamics of the mean field model represented by phase portraits (black circles are stable fixed points) for the two-member system (up) and the three-member hypercycle (down) in the all-species coexistence scenario (see Section 2). (c) Schematic diagram of the spatial dynamics simulated with cellular automata models. Here we display the microscopic structure of an alkali feldspar mineral surface (image obtained from [37]) and the spatial domain (i.e., a two-dimensional lattice, Γ) used for the simulations. The state-transition rules for the two-member hypercycle with the auto-catalytic short-circuit are displayed. Replicators can interact and reproduce, can be degraded, and can diffuse along the sites in Γ.

Alternatively, it could be possible that well-mixed hypercycles with short-circuits displayed stable coexistence, depending on the kinetic constants. Moreover, the exclusion of short-circuits driven by spatio-temporal phenomena has been described in hypercycles able to self-organize in rotating spiral waves, behavior that usually appears in hypercycles with five or more species (see e.g., [33,35]). However, the effect of short-circuits in smaller spatial hypercycles not able to form large-scale spatial structures have not been investigated. Such questions, crucial in early, small hypercycles remain thus unexplored. In this sense, a full description of the dynamics and transitions (i.e., bifurcations) in hypercycles with short-circuits seems necessary in order to hypothesize how these catalytic systems could circumvent this problem. Also, a comparison between the well-mixed system and the spatial counterpart seems necessary to reveal if space promotes small hypercycles with resistance to the short-circuits, as has been suggested in [35].

In this contribution we will focus on the dynamics of the smallest hypercycles with short-circuits. Here, by short-circuit we mean an inner closed cycle in which a given species establishes a single catalytic connection with another species (or with itself) inside a larger catalytic cycle, see Fig. 1(a). To do so, we will investigate a particular hypothetical scenario in the origin of life formed by small systems of catalytically-connected ribozymes. Our scenario considers the presence of small functional RNA molecules able to promote the replication of other molecules that are not able to replicate without the catalytic support. This might correspond, for example, to a scenario where ligase reactions in a given replicator might depend on the catalytic activity of another different template. We are interested in exploring the impact of short-circuits in these primordial systems and their role in the bifurcations (transitions) between phases. We will first investigate a two-species hypercycle that contains an auto-catalytic replicator as the minimal catalytic system with a short-circuit. Then, we will explore a three-member hypercycle that contains the previous system. The three-member system, albeit we are not explicitly modeling its formation from the two-member system, could arise from the growth (by means of replication and mutation) of the two-member one. Finally, we will quantify the likelihood of survival of the different catalytic cycles in the parameter space, comparing the outcomes of the well-mixed and the spatial systems.

2. Mean field model

We consider two minimal hypercycle systems with short-circuits. First, we will investigate a two-member hypercycle where one of the replicators is auto-catalytic. Then, we will extend this system to a three-member hypercycle by adding another species to the two-member architecture, see Fig. 1(a). Notice that our systems only consider auto- and hetero-catalytic interactions, and the species are not able to reproduce alone i.e., in a Malthusian way. Hence, our systems are similar to Kauffman's model of catalytic networks [30]. In our case we study the population dynamics of purely catalytic small networks, assuming an early appearance of short-circuits that could limit a stable persistence of the whole hypercycle. A model can be obtained for the three-member hypercycle (and the two-member one, see below), from:

$$\dot{x}_1 = x_1\left(k_{11}x_1 + k_{12}x_2 + k_{13}x_3\right)\theta(x) - \varepsilon x_1, \tag{1}$$

$$\dot{x}_2 = x_2\left(k_{21}x_1\right)\theta(x) - \varepsilon x_2, \tag{2}$$

$$\dot{x}_3 = x_3\left(k_{32}x_2\right)\theta(x) - \varepsilon x_3, \tag{3}$$

where $\theta(x) = 1 - (x_1 + x_2 + x_3)$ is a logistic growth term that introduces competition between the hypercycle elements. For short, we will also write system (1)–(3) as

$$\dot{x} = F(x), \quad x = (x_1, x_2, x_3).$$

The variables $x_i \geq 0$, $i = 1, 2, 3$, are the population numbers of the hypercycle species S_i (e.g., small ribozymes). The parameters $k_{ij} > 0$ (also with $j = 1, 2, 3$ and $j \neq i$) are the hetero-catalytic replication constants, i.e., the rate of replication of species i due to the catalytic aid from replicator j. Constant $k_{11} > 0$ denotes, as we previously mentioned, the constant of auto-catalytic growth of species S_1. Finally, the parameter $\varepsilon > 0$ represents the density-independent degradation rates of the species, which is taken to be equal in all species for the sake of simplicity. We emphasize that k_{ij} and ε will be kept strictly positive. Notice that the dynamical system for the two-member hypercycle with the auto-catalytic

species can be obtained from system (1)–(3) setting $x_3 = 0$. Defining

$$A = \begin{pmatrix} k_{11} & k_{12} & k_{13} \\ k_{21} & 0 & 0 \\ 0 & k_{32} & 0 \end{pmatrix} \quad \text{and} \quad D(x) = \begin{pmatrix} x_1 & 0 & 0 \\ 0 & x_2 & 0 \\ 0 & 0 & x_3 \end{pmatrix},$$

the system above can be written as $\dot{x} = F(x) = \theta(x)D(x)Ax - \varepsilon x$. It is clear from the equations that (0, 0, 0) is a fixed point and that the coordinate planes $\{x_j = 0\}$, for $j = 1, 2, 3$, are invariant. As a consequence, no solutions can cross such planes.

The system has biological meaning for non-negative values of the variables x_j. Moreover, any solution in that domain will enter into

$$\Omega = \left\{x \in \mathbb{R}^3 \mid x_1 \geq 0,\ x_2 \geq 0,\ x_3 \geq 0,\ x_1 + x_2 + x_3 \leq 1\right\}$$

and remains in Ω forever. Indeed, let $\phi(x) = x_1 + x_2 + x_3$ and compute the scalar product $F \cdot \operatorname{grad}\phi$ for $x_j \geq 0, x_1 + x_2 + x_3 = \delta$, with $\delta > 0$. We have

$$F \cdot \operatorname{grad}\phi = (x_1 (k_{11}x_1 + k_{12}x_2 + k_{13}x_3) + x_2 k_{21} x_1 + x_3 k_{32} x_2)\,\theta(x) - \varepsilon(x_1 + x_2 + x_3).$$

If $\delta \geq 1, \theta(x) \leq 0$ and hence $F \cdot \operatorname{grad}\phi \leq -\varepsilon\delta$ which means that the solutions must cross transversally all the planes $\{x_1 + x_2 + x_3 = \delta\}$ with $\delta \geq 1$, and finally enter into Ω.
Therefore we consider system (1)–(3) on the domain Ω since it contains the long-term behavior and the interesting dynamics.

2.1. Equilibrium points

As we have already mentioned the origin is always an equilibrium point and it is stable since $\varepsilon > 0$. Thus, we concentrate on the nontrivial equilibrium points of system (1)–(3) in the domain Ω, which we classify in terms of the parameters. We introduce some definitions to simplify the notation in the forthcoming computations:

$$\begin{aligned} &\alpha_2 := \frac{k_{21} - k_{11}}{k_{12}}, \qquad \alpha_3 := \frac{k_{21}}{k_{32}}, \\ &\beta_3 := \frac{k_{12}}{k_{13}}\left(\frac{k_{21} - k_{11}}{k_{12}} - \frac{k_{21}}{k_{32}}\right), \\ &\mu_2 := 1 + \alpha_2, \qquad \mu_3 := 1 + \alpha_3 + \beta_3, \\ &\Delta := \left(1 - \frac{k_{11}}{k_{21}}\right)^2 - 4\left(1 - \frac{k_{12}}{k_{32}}\right), \\ &\varepsilon_1 := \frac{k_{11}}{4}, \qquad \varepsilon_2 := \frac{k_{21}}{4\mu_2}, \qquad \varepsilon_3 := \frac{k_{21}}{4\mu_3}. \end{aligned} \tag{4}$$

Note that it follows straightforwardly from these definitions that $\beta_3 = \frac{k_{12}}{k_{13}}(\alpha_2 - \alpha_3)$ and that

$$\alpha_2 > 0 \iff k_{11} < k_{21}, \qquad \beta_3 > 0 \iff \frac{k_{11}}{k_{21}} + \frac{k_{12}}{k_{32}} < 1. \tag{5}$$

Proposition 1. *System (1)–(3) admits the following equilibrium points in Ω:*

(i) *Equilibrium points of type $(x_1, 0, 0)$ exist if and only if $\varepsilon \leq \varepsilon_1$, and in that case they are given by*

$$\begin{cases} P^{\pm} = (p_1^{\pm}, 0, 0) & \text{if } 0 < \varepsilon < \varepsilon_1, \\ P^0 = (p_1^0, 0, 0) & \text{if } \varepsilon = \varepsilon_1, \end{cases} \tag{6}$$

where $p_1^{\pm,0}$ are the two solutions of $\xi^2 - \xi + \varepsilon/k_{11} = 0$, that is,

$$p_1^{\pm} = \frac{1}{2}\left(1 \pm \sqrt{1 - \frac{\varepsilon}{\varepsilon_1}}\right), \quad \text{and} \quad p_1^0 = \frac{1}{2}. \tag{7}$$

(ii) *Equilibrium points of the form $(x_1, x_2, 0)$ exist in Ω if and only if $\varepsilon \leq \varepsilon_2$ and $k_{11} \leq k_{21}$ (equivalently, $\alpha_2 \geq 0$). In this case, they are given by*

$$\begin{cases} Q^{\pm} = (q_1^{\pm}, q_2^{\pm}, 0) & \text{if } 0 < \varepsilon < \varepsilon_2, \\ Q^0 = (q_1^0, q_2^0, 0) & \text{if } \varepsilon = \varepsilon_2, \end{cases} \tag{8}$$

where $q_1^{\pm}$ are the two solutions of $\mu_2\xi^2 - \xi + \varepsilon/k_{21} = 0$, that is,

$$q_1^{\pm} = \frac{1}{2\mu_2}\left(1 \pm \sqrt{1 - \frac{\varepsilon}{\varepsilon_2}}\right), \qquad q_1^0 = \frac{1}{2\mu_2}, \quad \text{and}$$
$$q_2^{\pm,0} = \alpha_2 q_1^{\pm,0}. \tag{9}$$

In the case that $k_{11} = k_{21}$ we have $\alpha_2 = 0$ and $\mu_2 = 1$. Consequently, $\varepsilon_2 = \varepsilon_1$ and therefore $Q^{\pm} = P^{\pm}$ and $Q^0 = P^0$. If $k_{11} > k_{21}$ (that is, $\alpha_2 < 0$) there are no fixed points of this type in Ω.

(iii) *Equilibrium points of the form (x_1, x_2, x_3) exist in Ω if and only if $\varepsilon \leq \varepsilon_3$ and $(k_{11}/k_{21}) + (k_{12}/k_{32}) \leq 1$ (equivalently, $\beta_3 \geq 0$). In this case, they are given by*

$$\begin{cases} R^{\pm} = (r_1^{\pm}, r_2^{\pm}, r_3^{\pm}) & \text{if } 0 < \varepsilon < \varepsilon_3 \\ R^0 = (r_1^0, r_2^0, r_3^0) & \text{if } \varepsilon = \varepsilon_3, \end{cases}$$

where $r_1^{\pm}$ are the two solutions of $\mu_3\xi^2 - \xi + \varepsilon/k_{21} = 0$, that is,

$$r_1^{\pm} = \frac{1}{2\mu_3}\left(1 \pm \sqrt{1 - \frac{\varepsilon}{\varepsilon_3}}\right), \quad r_1^0 = \frac{1}{2\mu_3} \quad \text{and}$$
$$r_2^{\pm,0} = \alpha_3 r_1^{\pm,0}, \qquad r_3^{\pm,0} = \beta_3 r_1^{\pm,0}.$$

In the case that $(k_{11}/k_{21}) + (k_{12}/k_{32}) = 1$ (i.e. $\beta_3 = 0$) we have $\mu_3 = \mu_2$, $\varepsilon_3 = \varepsilon_2$ and therefore $R^{\pm} = Q^{\pm}$ and $R^0 = Q^0$. On the contrary, if $(k_{11}/k_{21}) + (k_{12}/k_{32}) > 1$ (that is $\beta_3 < 0$) there are no fixed points of this type in the domain Ω.

The proof of the proposition is elementary and has been omitted. The stability of these equilibria is provided by Proposition 2. In Figs. 2 and 3 we show the relative positions of points $P^{\pm,0}$, $Q^{\pm,0}$ and $R^{\pm,0}$. For the sake of clarity, in Fig. 2, we only show the evolution of the first coordinate of $P^{\pm,0}$ and $Q^{\pm,0}$ in terms of the parameter ε. It is worth noticing the straightforward relation

$$4(\varepsilon_2 - \varepsilon_1) = (k_{21} - k_{11})(k_{12} - k_{11})/(k_{21} + k_{12} - k_{11}), \tag{10}$$

which implies, under the hypothesis of existence of $Q^{\pm,0}$ ($k_{21} > k_{11}$), that $\operatorname{sign}(\varepsilon_2 - \varepsilon_1) = \operatorname{sign}(k_{12} - k_{11})$. Panels (a–c) in Fig. 2 illustrate the three different possibilities of $\operatorname{sign}(\varepsilon_2 - \varepsilon_1)$.

We also want to emphasize that the condition $k_{11} > k_{21}$ does not lead to a disappearance of equilibria $Q^{\pm,0}$ but to the negativity of the second component, which does not make sense, biologically, in our model. In Fig. 4 we show both the collision of points $P^{\pm,0}$ with the homologous $Q^{\pm,0}$ that occurs when $k_{11} = k_{21}$ (panel (a)) and the coincidence of the first coordinates of $P^{\pm,0}$ and $Q^{\pm,0}$ together with the vanishing of $q_2^{\pm,0}$ (panel (b)). In Section 2.3, we further explore this seeming bifurcation. Similar comments are applicable to the condition $(k_{11}/k_{21}) + (k_{12}/k_{32}) < 1$ and the points $Q^{\pm,0}$ and $R^{\pm,0}$. The biological implications of these observations are commented in the next remark.

Another way to visualize the evolution of points $Q^{\pm}$, that will be complemented in Section 2.3 when we study bifurcations, is given in Fig. 5, where we show the number of equilibria on the (k_{11}, k_{21})-plane. On this plane, the condition $\varepsilon = \varepsilon_2$ beyond which the points $Q^{\pm}$ vanish writes as $k_{21} = 4\varepsilon\,(k_{12} - k_{11})/(k_{12} - 4\varepsilon)$.

Remark 1. Notice that in order to have nontrivial equilibria $Q^{\pm,0}$ the condition to be satisfied is $k_{11} < k_{21}$, that is, auto-catalysis needs to be weaker than hetero-catalysis. In other words, the

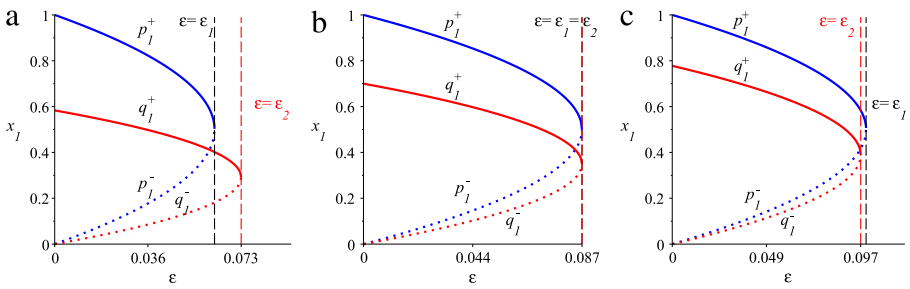

Fig. 2. Position of the first coordinate of the fixed points P^+, Q^+ (solid lines) and P^-, Q^- (dotted lines) when moving ε from 0 to ε_1 and ε_2, respectively. The three panels show different relations among the parameters. (a) Case $\varepsilon_1 < \varepsilon_2$; we use the set $k_{11} = 0.25$, $k_{12} = 0.35$, $k_{21} = 0.5$; (b) case $\varepsilon_1 = \varepsilon_2$; we use the set $k_{11} = k_{12} = 0.35$, $k_{21} = 0.5$; (c) case $\varepsilon_1 > \varepsilon_2$: $k_{11} = 0.4$, $k_{12} = 0.35$, $k_{21} = 0.5$.

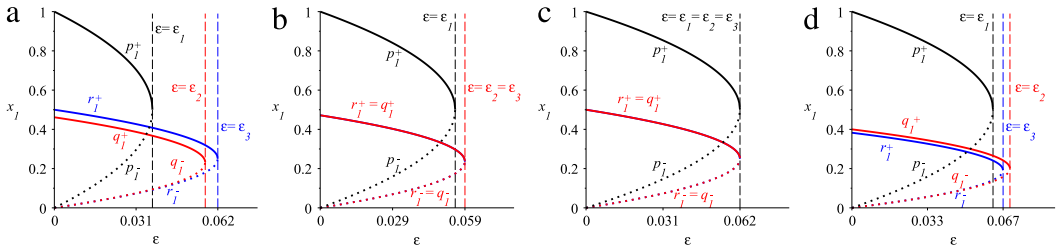

Fig. 3. Equilibrium points for different relations among parameters. (a) $\varepsilon_1 < \varepsilon_2 < \varepsilon_3$. We use the set of parameters $k_{11} = 0.15$, $k_{12} = 0.3$, $k_{21} = 0.5$, $k_{13} = 0.45$, $k_{32} = 0.75$. Observe that $k_{12} < k_{13}$ and $k_{11} < k_{12}$. (b) $\varepsilon_1 < \varepsilon_2 = \varepsilon_3$. Setting the parameters to $k_{11} = 0.22$, $k_{12} = 0.25$, $k_{21} = 0.5$, $k_{13} = 0.25$, $k_{32} = 0.75$. Notice that $k_{12} = k_{13}$ and $k_{11} < k_{12}$. (c) $\varepsilon_1 = \varepsilon_2 = \varepsilon_3$. Using $k_{11} = 0.25$, $k_{12} = 0.25$, $k_{21} = 0.5$, $k_{13} = 0.25$, $k_{32} = 0.75$. Here $k_{11} = k_{12} = k_{13}$. (d) $\varepsilon_1 < \varepsilon_3 < \varepsilon_2$. Fixing now $k_{11} = 0.25$, $k_{12} = 0.3$, $k_{21} = 0.5$, $k_{13} = 0.25$, $k_{32} = 0.75$. Observe that $k_{12} > k_{13}$ and $k_{11} < k_{12}$.

hypercycle must dominate over the inner short-circuit. On the other hand, the condition to have the equilibria $R^{\pm,0}$, namely $k_{11}/k_{21} + k_{12}/k_{32} < 1$, implies, in particular, that $k_{11}/k_{21} < 1$ and $k_{12}/k_{32} < 1$. In biological terms, the second inequality means that species S_2 must invest more in the 3-hypercycle than in the former hypercycle of two species to maintain the nontrivial equilibria with population S_3 active. Taking into account the whole inequality, we appreciate that the existence of these nontrivial points implies also a balance between the two restrictions: if the auto-catalytic activity in S_1 is close to the catalysis activity from S_1 to S_2, then the catalysis from S_2 to S_1 must be very weak compared to the catalysis from S_2 to S_3, and vice versa.

2.2. Invariant lines and stability

Determining the invariant lines of system (1)–(3) is very useful in our study: first, because of its dynamical consequences; second, and not less important, because they help in the computation of the eigenvectors and eigenvalues of the equilibrium points which are located on them.

The next result establishes which are these invariant lines.

Lemma 1. *System (1)–(3) has the following invariant lines through the origin.*

(i) $L_1 = \{tv_1 \mid t \in \mathbb{R}\}$, *with* $v_1 = (1, 0, 0)$.
(ii) $L_2 = \{tv_2 \mid t \in \mathbb{R}\}$, *with* $v_2 = (1, \alpha_2, 0)$ *and* α_2 *as defined in (4).*
(iii) $L_3 = \{tv_3 \mid t \in \mathbb{R}\}$, *with* $v_3 = (1, \alpha_3, \beta_3)$ *and* α_3, β_3 *as defined in (4).*
(iv) $L_j = \{tv_j \mid t \in \mathbb{R}\}$, $j = 4, 5$, *with* $v_4 = (0, 1, 0)$ *and* $v_5 = (0, 0, 1)$.
(v) $L_6 = \{tv_6 \mid t \in \mathbb{R}\}$, *with* $v_6 = (1, 0, \beta_6)$ *and* $\beta_6 = -k_{11}/k_{13} < 0$.

Moreover, each equilibrium point is on one of these lines. We also have

- L_2 *intersects* $\Omega \setminus \{0\}$ *if and only if* $k_{21} \geq k_{11}$ *or, equivalently,* $\alpha_2 \geq 0$. *If* $k_{21} = k_{11}$ *then* $L_2 = L_1$.

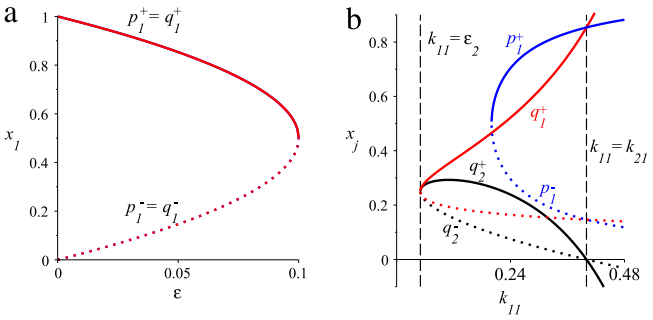

Fig. 4. Case $k_{11} = k_{21}$. (a) Evolution of the first coordinate of the fixed points P^+, Q^+ (solid lines) and P^-, Q^- (dotted lines) when moving ε from 0 to ε_1 and ε_2, respectively. We use $k_{11} = k_{21} = 0.4$, $k_{12} = 0.35$, which implies $\mu_2 = 1$ and, therefore $\varepsilon_1 = \varepsilon_2$. (b) Plot of the first coordinate of $P^{\pm,0}$, and the first and second coordinates of $Q^{\pm,0}$ in terms of k_{11}. Note that $p_1^{\pm,0} = q_1^{\pm,0}$ and $q_2^{\pm,0} = 0 (< 0)$ for $k_{11} = k_{21}$ ($k_{11} > k_{21}$).

- L_3 *intersects* $\Omega \setminus \{0\}$ *if and only if* $\beta_3 \geq 0$. *If* $\beta_3 = 0$ *then* $L_3 = L_2$. *If* $\alpha_2 = \beta_3 = 0$ *then* $L_1 = L_2 = L_3$.
- L_6 *never intersects* $\Omega \setminus \{0\}$.

Proof. We evaluate the vector field F at the points of the line tv for some unknown vector v and we look for v such that on this line the vector field has the direction of v, that is $F(tv) \propto v$. We begin by looking for v of the form $v = (1, \alpha, \beta)$. The proportionality condition reads

$$F(tv) = t \begin{pmatrix} ((k_{11} + \alpha k_{12} + \beta k_{13})(1 - (1 + \alpha + \beta)t)t - \varepsilon) \\ \alpha\,(k_{21}(1 - (1 + \alpha + \beta)t)t - \varepsilon) \\ \beta\,(\alpha k_{32}(1 - (1 + \alpha + \beta)t)t - \varepsilon) \end{pmatrix} \propto \begin{pmatrix} 1 \\ \alpha \\ \beta \end{pmatrix}. \tag{11}$$

- If $\alpha = 0$ and $\beta = 0$, v has to be a multiple of $v_1 = (1, 0, 0)$.
- If $\alpha \neq 0$ and $\beta = 0$ the condition (11) implies $k_{11} + \alpha k_{12} = k_{21}$, which gives (ii).

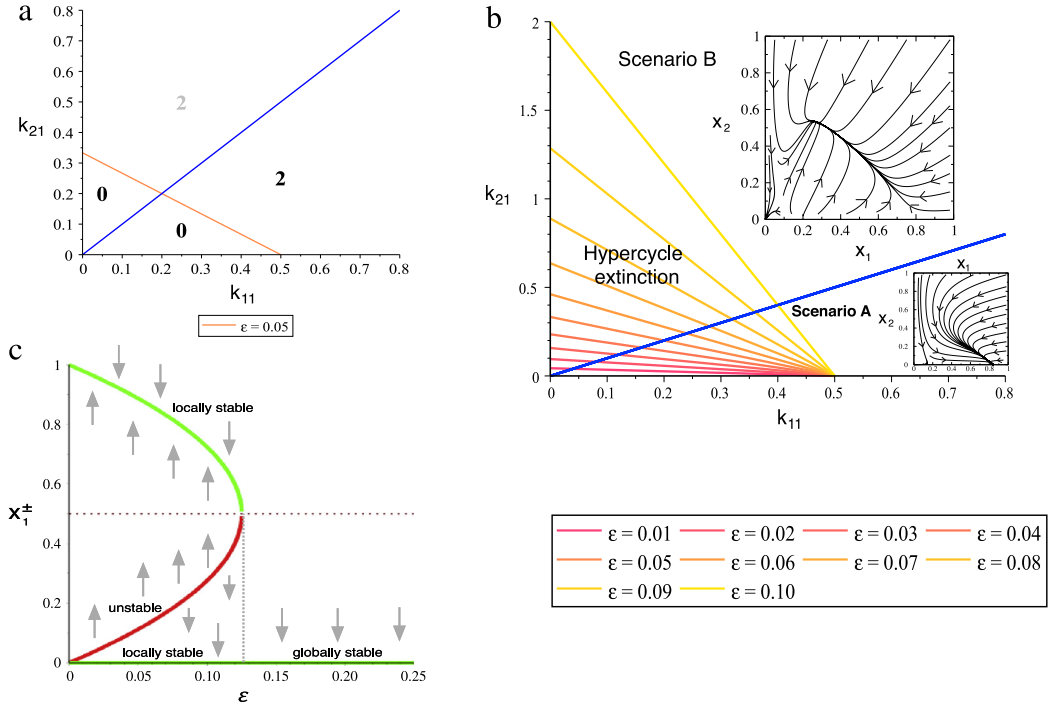

Fig. 5. Representation, on the (k_{11}, k_{21}) plane, of the existence of points $Q^{\pm}$ in Proposition 1(ii). The other parameters are kept constant: $k_{12} = 0.5$, $k_{13} = 0.5$, $k_{32} = 0.95$. (a) Number of fixed points for $\varepsilon = 0.05$. On the red line (with negative slope), a saddle–node bifurcation occurs; more precisely, this is the line given by $k_{21} = 4\,\varepsilon\,(k_{12} - k_{11})/(k_{12} - 4\,\varepsilon)$. The blue line (positive slope) is not a bifurcation curve indeed, but the line on which some component of $Q^{\pm}$ vanishes, thus losing its biological meaning. (b) Position of the saddle–node bifurcation line for different values of ε in the parameter space (k_{11}, k_{21}). The insets display possible dynamics tied to scenarios A and B (discussed in Section 3). Scenario A corresponds to the persistence of the auto-catalytic species alone, while scenario B corresponds to the persistence of the two-member hypercycle. (c) Stability diagram for the fixed points x_1^+ (upper branch), x_1^- (lower branch), and $x = 0$. Green color denotes *attractor* and red *repeller*. (For interpretation of the references to color in this figure legend, the reader is referred to the web version of this article.)

- If $\alpha \neq 0$ and $\beta \neq 0$ the condition (11) implies $k_{11} + \alpha k_{12} + \beta k_{13} = k_{21} = \alpha k_{32}$, which has the unique solution for α and β given in (iii).
- If $\alpha = 0$ and $\beta \neq 0$ the condition (11) implies $k_{11} + \beta k_{13} = 0$, which gives $\beta = -k_{11}/k_{13} < 0$. This provides an invariant line but it does not cut the interior of Ω.

Finally we look for v of the form $v = (0, \alpha, \beta)$. The proportionality condition now reads as

$$F(tv) = \begin{pmatrix} 0 \\ \alpha\,(-\varepsilon t) \\ \beta\left(-\varepsilon t + \alpha k_{32} t^2 (1 - (\alpha + \beta) t)\right) \end{pmatrix} \propto \begin{pmatrix} 0 \\ \alpha \\ \beta \end{pmatrix},$$

which gives the further invariant lines generated by $v_4 = (0, 1, 0)$ and $v_5 = (0, 0, 1)$. The statement concerning the equilibrium points follows from a direct check. □

We denote by $DF(x)$ the Jacobian matrix of F at a point x.

Proposition 2. *Consider the equilibrium points $P^{\pm,0}$, $Q^{\pm,0}$ and $R^{\pm,0}$ described in Proposition 1. Then:*

(i) *The eigenvalues $\lambda_j^{\pm,0}$ of DF at the points $P^{\pm,0}$ are given by*

$$\lambda_1^{\pm} = 2k_{11}p_1^{\pm}\left(\frac{1}{2} - p_1^{\pm}\right), \qquad \lambda_2^{\pm} = \frac{k_{21} - k_{11}}{k_{11}}\varepsilon,$$
$$\lambda_3^{\pm} = -\varepsilon < 0.$$

Moreover, $\lambda_1^+ < 0$ and $\lambda_1^- > 0$. In particular, at the point P^0, the eigenvalues become $\lambda_1^0 = 0$, $\lambda_2^0 = (k_{21} - k_{11})/4$ and $\lambda_3^0 = -\varepsilon_1 < 0$.

(ii) *The equilibrium points $Q^{\pm,0}$ lie on the invariant line L_2 and $v_2 = (1, \alpha_2, 0)$ is an eigenvector of DF. The eigenvalues $\lambda_j^{\pm,0}$ of DF at the points $Q^{\pm,0}$ are:*

$$\lambda_1^{\pm,0} = \frac{k_{13}}{k_{12}}\frac{\beta_3}{\alpha_3}\varepsilon, \qquad \lambda_2^{\pm,0} = \varepsilon - k_{21}\mu_2\left(q_1^{\pm,0}\right)^2,$$
$$\lambda_3^{\pm,0} = -\alpha_2\varepsilon < 0,$$

where $q_1^{\pm,0}$ is the first component of $Q^{\pm,0}$, respectively. In particular, $\operatorname{sign}(\lambda_1^{\pm,0}) = \operatorname{sign}(\beta_3)$; $\lambda_2^+ < 0$, $\lambda_2^- > 0$ and $\lambda_2^0 = 0$; and $\lambda_3^{\pm,0} < 0$.

In the case $k_{11} = k_{21}$ the points $Q^{\pm,0}$ coincide with the points $P^{\pm,0}$.

(iii) *The equilibrium points $R^{\pm,0}$ lie on the invariant line L_3 and $v_3 = (1, \alpha_3, \beta_3)$ is an eigenvector of DF. The eigenvalues $\lambda_j^{\pm,0}$ of DF at the points $R^{\pm,0}$ are given by:*

$$\lambda_1^{\pm,0} = \varepsilon - \mu_3 k_{21}\left(r_1^{\pm,0}\right)^2,$$
$$\lambda_2^{\pm,0} = -\frac{1}{2}\left(1 - \frac{k_{11}}{k_{21}}\right) + \frac{\varepsilon}{2}\sqrt{\Delta},$$
$$\lambda_3^{\pm,0} = -\frac{1}{2}\left(1 - \frac{k_{11}}{k_{21}}\right) - \frac{\varepsilon}{2}\sqrt{\Delta}.$$

Moreover, $\lambda_1^+ < 0$, $\lambda_1^- > 0$, $\lambda_1^0 = 0$, $\lambda_{2,3}^{\pm} < 0$ if $\Delta \geq 0$, and $\operatorname{Re}\lambda_{2,3}^{\pm} < 0$ if $\Delta < 0$.

In the case $(k_{11}/k_{21}) + (k_{12}/k_{32}) = 1$ the points $R^{\pm,0}$ coincide with $Q^{\pm,0}$.

The proof of this proposition has been deferred to Appendix.

2.3. Bifurcations

In this section we use the information provided by Propositions 1 and 2 to identify the different bifurcations and scenarios of stability in the space of parameters. We focus on the

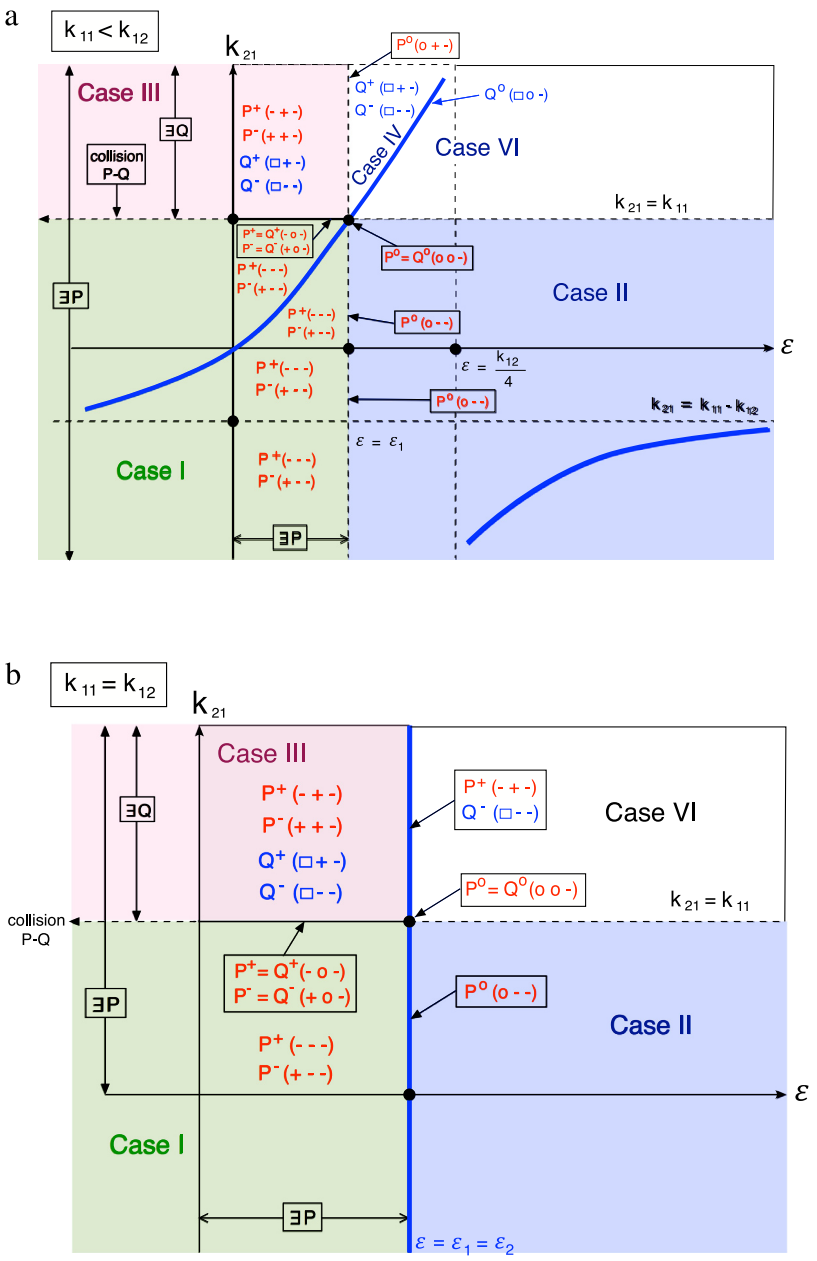

Fig. 6. PQ-bifurcation 2-dimensional diagrams. The diagrams show (i) the regions of existence and non-existence of the equilibrium points $P^{\pm,0}$ and $Q^{\pm,0}$ together with (ii) the signs of the three (real) eigenvalues of the associated Jacobian matrix. The bifurcation curves appearing correspond to a pass through 0 of one or more of these eigenvalues. Observe that the appearance of equilibria $R^{\pm,0}$, related to $\beta_3 > 0$, causes a change in the stability of the points Q^-. The sign (β_3) has been denoted by □ in the diagram. The cases, represented with different colors, correspond to those listed in Table 1. From top to bottom, (a) $k_{11} < k_{12}$ and (b) $k_{11} = k_{12}$. (For interpretation of the references to color in this figure legend, the reader is referred to the web version of this article.)

2-dimensional space, the minimal dimension in which the most interesting bifurcation types appear. As stated above, the dynamics of the two-member hypercycle with the short-circuit is described by system (1)–(2) with $x_3 = 0$. In terms of parameters k_{11}, k_{12}, k_{21} and ε, we have the cases given in Table 1.

We note that bifurcations of equilibria in Ω are due to two reasons: either a saddle–node bifurcation when ε overcomes the thresholds ε_1 and ε_2, or a transcritical bifurcation that makes at least one equilibrium to leave Ω and switch its stability character. According to Table 1, these events occur whenever we have an equality (we mean, in $k_{21} - k_{11}$ or in ε). The number of equalities that meet simultaneously correspond to the so-called *codimension* of the bifurcation.

In Figs. 6 and 7, we illustrate all these bifurcations on the plane (ε, k_{21}) (degradation rate and catalysis from population 1 to population 2, respectively). The bifurcation diagram is shown on the four quadrants although only the first one makes sense in our model (since $\varepsilon_2, k_{21} > 0$). For the sake of clarity, we have divided the figures in three panels: in Fig. 6 we represent the cases (a) $k_{11} < k_{12}$, (b) $k_{11} = k_{12}$ and, in Fig. 7, we display the case $k_{11} > k_{12}$. We remind that the sign of $k_{12} - k_{11}$ is equivalent to the sign of $\varepsilon_2 - \varepsilon_1$ as seen in (10). On these panels, we plot the bifurcation curves identified in Table 1. Both $\varepsilon = \varepsilon_1$ and $k_{21} = k_{11}$ are straight lines on this plane and correspond, respectively, to the locus where the saddle–node bifurcation of points $P^{\pm}$ and the transcritical bifurcation occur. The curve where the points $Q^{\pm}$ collide, $\varepsilon = \varepsilon_2$, becomes a rational function in terms of k_{21} (see the blue curves in the figures):

$$\varepsilon_2(k_{21}) := \frac{k_{21}\, k_{12}}{4\,(k_{21} + k_{12} - k_{11})}.$$

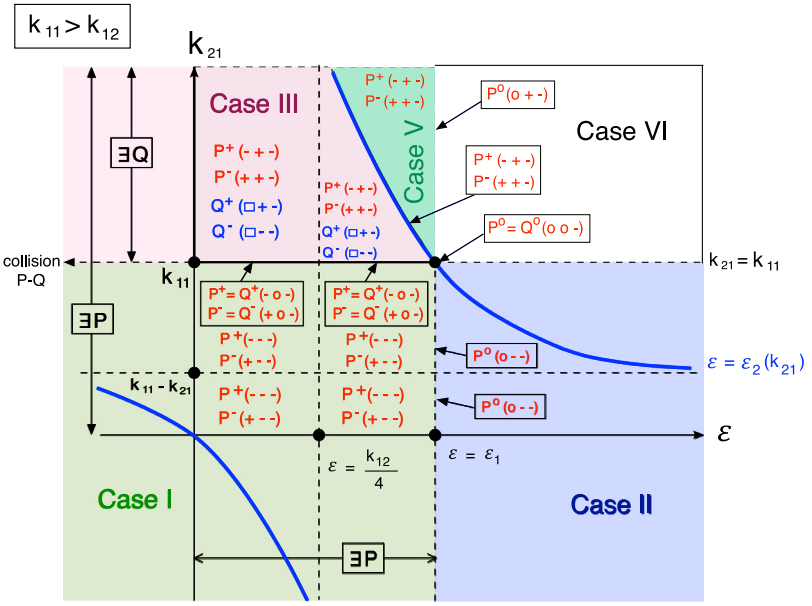

Fig. 7. *PQ*-bifurcation 2-dimensional diagrams. Same situation as presented in Fig. 6 but in the case $k_{11} > k_{12}$. We remind that the symbol □ denotes sign(β_3) and that the cases represented with different colors correspond to those listed in Table 1. (For interpretation of the references to color in this figure legend, the reader is referred to the web version of this article.)

Observe that $\varepsilon_2(k_{11}) = k_{11}/4$ and that $\varepsilon_2(k_{21})$ is asymptotic to the lines $\varepsilon = k_{12}/4$ and $k_{21} = k_{11} - k_{12}$.

On the different regions determined by all these bifurcation curves, the existing $P^{\pm,0}$, $Q^{\pm,0}$ points have been written. Aside each equilibrium point $P^{\pm,0}$ or $Q^{\pm,0}$, triplets with symbols denote the signs of the corresponding eigenvalues, which are always real; for instance, $(+\,0\,-)$ would indicate $\lambda_1 > 0$, $\lambda_2 = 0$ and $\lambda_3 < 0$. The eigenvalues of $Q^{\pm,0}$ depend as well on β_3, which involves other parameters; the stability notation, thus, also considers this circumstance.

In Figs. 6 and 7, the cases described in Table 1 have been overlayed as well. This allows to match these classes with the above described bifurcations. For instance, transitions from case I to case II (see Figs. 6(a), (b) and 7), from III to IV (see Fig. 6(a)) or from V to VI (see Fig. 7), induce a saddle–node bifurcation involving the equilibria $P^{\pm}$ that merge into P^0 when $\varepsilon = \varepsilon_1$ and then disappear. Analogous bifurcations occur for equilibria $Q^{\pm,0}$ when $\varepsilon = \varepsilon_2$ from IV to VI (see Fig. 6(a)) or from III to V (see Fig. 7).

On the other hand, equilibria $Q^{\pm}$ undergo transcritical bifurcations when $k_{21} = k_{11}$, that is, from III to I (see Figs. 6(a), (b) and 7). In these cases, the second component of $Q^{\pm}$, i.e. $q_2^{\pm}$, becomes negative (see Fig. 4(b)) thus leaving Ω and, at the same time, one eigenvalue changes sign. Depending on the sign of β_3, the transcritical "exchange" is made with points $P^{\pm}$ or $R^{\pm}$.

All other bifurcations are, at least, of codimension two. For instance, when $\varepsilon = \varepsilon_1 = \varepsilon_2$ or the two conditions $\varepsilon = \varepsilon_1$ and $k_{11} = k_{21}$ hold simultaneously, as those observed from III to VI (see Fig. 6(b)) and from IV to V (moving from Fig. 6(a) to Fig. 7).

The analysis of bifurcations in the phase space (x_1, x_2, x_3) becomes more cumbersome just because of the increase in the number of parameters and conditions to be taken into account, but it does not show other codimension-1 bifurcations qualitatively different from those described in the phase space (x_1, x_2). More precisely, in the 3D case we have to take into account the new parameters k_{13} and k_{23} and the conditions $k_{11}/k_{21} + k_{12}/k_{32} = 1$ (related to the transcritical bifurcation between points $R^{\pm}$ and points $Q^{\pm}$) and $\varepsilon = \varepsilon_3$ (saddle–node bifurcation of points $R^{\pm}$). We think that these comments give already a fair idea of the bifurcations in the three dimensional case, so to avoid unnecessary intricacy in the manuscript we do not present the exhaustive study of bifurcations in this case. Fig. 15 in the Appendix Section includes a biparametric diagram displaying the different dynamics for the three-member hypercycle in terms of parameters k_{11}/k_{21} and k_{12}/k_{32}.

2.4. Non-existence of periodic orbits

In this section we will explore both analytically and numerically whether periodic orbits (stable or unstable) can be found in the parameter space of the models.

2.4.1. Two-member system

The two-member system can be seen as the three-member system restricted to $\{x_3 = 0\}$, which is invariant. We denote by F_{12} the vector field F restricted to $\{x_3 = 0\}$. We take as domain of F_{12} the set

$$\Omega_2 = \Omega \cap \{x_3 = 0\} = \{(x_1, x_2) \mid x_1 \geq 0,\ x_2 \geq 0,\ x_1 + x_2 \leq 1\}\,.$$

Note that, in the same way as in the three-member system, the solutions in $\{(x_1, x_2) \mid x_1 \geq 0,\ x_2 \geq 0\}$ enter into Ω_2 and then remain there because Ω_2 is positively invariant. We have the following properties

Proposition 3. (i) *The vector field F_{12} has no periodic orbits in Ω_2.*
(ii) *The origin is a global attractor for F_{12} in Ω_2 if and only if either $k_{21} \leq k_{11}$ and $\varepsilon > \varepsilon_1$ or $k_{21} > k_{11}$ and $\varepsilon > \max\{\varepsilon_1, \varepsilon_2\}$.*

Proof. Since F_{12} is a planar vector field we can easily prove (i) using the Poincaré–Bendixson theorem. We already know that the domain Ω_2 is positively invariant. Let $(x_1, x_2) \in \Omega_2$ and consider its ω-limit. It must be an equilibrium point, a periodic orbit or a graph formed by equilibrium points and homo/heteroclinic orbits connecting them. If there is a periodic orbit, by a Poincaré–Hopf theorem there should be an equilibrium point inside it, but this possibility cannot happen in our case since all equilibrium points are contained in invariant lines, and then the periodic orbit should intersect one of such invariant lines. This is impossible by uniqueness of solutions.

From Proposition 1 we know that the conditions in (ii) imply that F_{12} has no equilibrium points in Ω_2 except the origin. Then the ω-limit set of every solution must be the origin.

Table 1
Existence and stability of equilibria in Ω in the planar case. Each case is displayed in the parameter spaces of Figs. 6 and 7 with different colors: Case I (light green); II (blue); III (pink); IV (white, Fig. 6(a)); V (dark green); and VI (white).

Case	$k_{21}-k_{11}$	ε	P^-	P^+	Q^-	Q^+
I	<0	$\varepsilon<\varepsilon_1$	Saddle	Attractor	$\nexists$	$\nexists$
II	<0	$\varepsilon>\varepsilon_1$	$\nexists$	$\nexists$	$\nexists$	$\nexists$
III	>0	$\varepsilon<\min\{\varepsilon_1,\,\varepsilon_2\}$	Saddle	Saddle	Saddle	Attractor
IV	>0	$\varepsilon_1<\varepsilon<\varepsilon_2$	$\nexists$	$\nexists$	Saddle	Attractor
V	>0	$\varepsilon_2<\varepsilon<\varepsilon_1$	Saddle	Saddle	$\nexists$	$\nexists$
VI	>0	$\varepsilon>\max\{\varepsilon_1,\,\varepsilon_2\}$	$\nexists$	$\nexists$	$\nexists$	$\nexists$

Conversely, if the conditions on the parameters do not hold there are other equilibrium points in Ω_2 and hence the origin cannot be a global attractor. □

2.4.2. Three-member system

Concerning the 3D system we provide a quite complete analytical description of the dynamics when $\beta_3 \le 0$. For $\beta_3 > 0$ we have to proceed numerically (numerical integrations along the work have been performed with a Runge–Kutta–Fehlberg (RKF78) method, with automatic step size control, using a step size $10^{-4} \le \Delta t \le 10^{-1}$ and the local relative tolerance 10^{-14}).

Proposition 4. *Assume $\beta_3 \le 0$. Then:*

(i) *The vector field F has no periodic orbits in Ω.*
(ii) *If either $k_{21} \le k_{11}$ and $\varepsilon > \varepsilon_1$ or $k_{21} > k_{11}$ and $\varepsilon > \max\{\varepsilon_1,\,\varepsilon_2\}$, the origin is a global attractor for F.*

Before proving Proposition 4 we state an auxiliary result. If $\alpha_2 > 0$ we introduce

$$\Omega^+_{\alpha_2} = \{x \in \Omega \mid x_2 \ge \alpha_2 x_1\}, \qquad \Omega^-_{\alpha_2} = \{x \in \Omega \mid x_2 < \alpha_2 x_1\}.$$

If $\alpha_2 \le 0$, for any $\eta > 0$ we introduce

$$\Omega^+_{\eta} = \{x \in \Omega \mid x_2 \ge \eta x_1\}, \qquad \Omega^-_{\eta} = \{x \in \Omega \mid x_2 < \eta x_1\}.$$

Clearly $\Omega = \Omega^+_{\alpha_2} \cup \Omega^-_{\alpha_2}$ and $\Omega = \Omega^+_{\eta} \cup \Omega^-_{\eta}$, respectively.

Lemma 2. (i) *If $\alpha_2 > 0$ then, given any initial condition in $\Omega^+_{\alpha_2}$, the solution enters into $\Omega^-_{\alpha_2}$ or converges to a fixed point in $\{x \in \Omega \mid x_2 = \alpha_2 x_1,\ x_3 = 0\}$.*
(ii) *If $\alpha_2 \le 0$ then, for any $\eta > 0$, given any initial condition in Ω^+_{η}, the solution enters into Ω^-_{η} or converges to a fixed point in $\{x \in \Omega \mid x_2 = 0,\ x_3 = 0\}$ if $\alpha_2 = 0$ or converges to the origin if $\alpha_2 < 0$.*

Proof. We recall that the coordinate axes are invariant and that Ω is positively invariant. We introduce the functions $\phi_\gamma(x) = -\gamma x_1 + x_2$ for $\gamma \ge \alpha_2$. The set $\{\phi_\gamma = 0\}$ represents a plane for which grad ϕ_γ is an orthogonal vector. We compute the scalar product $F \cdot \text{grad}\,\phi_\gamma$ on points of $\{\phi_\gamma = 0\} \cap (\Omega \setminus \partial\Omega)$ (in particular, points with strictly positive coordinates and such that $\theta(x) > 0$). We have

$$\begin{aligned} F \cdot \text{grad}\,\phi_\gamma &= -\gamma \dot{x}_1 + \dot{x}_2 \\ &= x_1\theta(x)\left(-\gamma\left(k_{11}x_1 + k_{12}x_2 + k_{13}x_3\right) + k_{21}x_2\right) \\ &= \gamma x_1 \theta(x)\left(\left(k_{21} - k_{11} - \gamma k_{12}\right)x_1 - k_{13}x_3\right) < 0. \end{aligned}$$

Notice that we have used that $\varepsilon(\gamma x_1 - x_2) = 0$ on $\{\phi_\gamma = 0\}$. The above inequality indicates that the solutions starting in $\Omega^+_{\alpha_2} \setminus \partial\Omega^+_{\alpha_2}$ cross all planes $\{\phi_\gamma = 0\}$, with $\gamma \ge \alpha_2 = (k_{21}-k_{11})/k_{12}$, transversally. In particular, $\Omega^-_{\alpha_2}$ is positively invariant. Then every solution either arrives at $\{\phi_{\alpha_2} = 0\} \cap \Omega \setminus \partial\left(\{\phi_{\alpha_2} = 0\} \cap \Omega\right)$ in which case it crosses this set transversally and enters into $\Omega^-_{\alpha_2}$ or tends to $\partial\left(\{\phi_\gamma = 0\} \cap \Omega\right)$ for some $\gamma \ge \alpha_2$. In the latter case the solution must follow the dynamics on this boundary (by continuity), which is one-dimensional and hence the solution converges to an equilibrium point laying on $\{x \in \Omega \mid x_2 = \alpha_2 x_1,\ x_3 = 0\}$.

If $\alpha_2 \le 0$ the previous computations also give that the solutions either arrive at $\{\phi_\eta = 0\} \cap \Omega$ and cross it transversally or go to $\partial\left(\{\phi_\eta = 0\} \cap \Omega\right)$. □

Proof of Proposition 4. (i) From Lemma 2 we know that the long term dynamics is in either $\Omega^-_{\alpha_2}$ if $\alpha_2 > 0$ or in Ω^-_{η}, for all $\eta > 0$, if $\alpha_2 \le 0$. Now we introduce $\psi_\gamma(x) = -\gamma x_2 + x_3$, for $\gamma > 0$, and we compute the scalar product $F \cdot \text{grad}\,\psi_\gamma$ on $\{\psi_\gamma = 0\} \cap \Omega^-_{\alpha_2}$ or $\{\psi_\gamma = 0\} \cap \Omega^-_{\eta}$. We have

$$\begin{aligned} F \cdot \text{grad}\,\psi_\gamma &= -\gamma\left(x_2 k_{21} x_1 \theta(x) - \varepsilon x_2\right) + x_3 k_{32} x_2 \theta(x) - \varepsilon x_3 \\ &= x_2\theta(x)\left(-\gamma k_{21} x_1 + x_3 k_{32}\right) \\ &= \gamma k_{32} x_2 \theta(x)\left(-\alpha_3 x_1 + x_2\right), \end{aligned}$$

where we have used that $\varepsilon(\gamma x_2 - x_3) = 0$ on $\{\psi_\gamma = 0\}$. Note that $\beta_3 \le 0$ is equivalent to

$$\alpha_2 = \frac{k_{21} - k_{11}}{k_{12}} \le \frac{k_{21}}{k_{32}} = \alpha_3.$$

Then, under this assumption,

$$F \cdot \text{grad}\,\psi_\gamma \le \gamma k_{32} x_2 \theta(x)\left(-\alpha_2 x_1 + x_2\right) < 0,$$

and hence a solution starting in $\Omega^-_{\alpha_2}$ must cross all planes $\{\psi_\gamma = 0\}$, $\gamma > 0$, and tend to $\{x_3 = 0\}$. Since in this plane there are no periodic orbits, as it is proved in Proposition 3, we conclude that there are no periodic orbits.

(ii) According to Lemma 1, the conditions on the parameters imply that F has a unique equilibrium point at the origin, which is asymptotically stable. By Proposition 3, the set $\{x \in \Omega \mid x_3 = 0\}$ is contained in the basin of attraction of the origin. Since the basin is an open set it also contains a set $\{x \in \Omega \mid 0 \le x_3 < \delta\}$ for some $\delta > 0$. In (i) we have proved that all solutions tend to $\{x_3 = 0\}$. Then they first enter into $\{x \in \Omega \mid 0 \le x_3 < \delta\}$ and then converge to the origin. □

When $\beta_3 > 0$ we have to deal with the non-existence of periodic orbits numerically. To facilitate the study we first provide some features of the dynamics. We introduce the planes through the origin generated by one of the coordinate axis and the vector $v_3 = (1, \alpha_3, \beta_3)$ which generates the line L_3, see Lemma 1. More precisely, let Π_i be the plane $\Pi_i = \{te_i + sv_3 \mid t, s \in \mathbb{R}\}$, where $\{e_i\}_i$ are the vectors of the canonical basis. These planes divide Ω into three subdomains $\Omega = \Omega_{12} \cup \Omega_{23} \cup \Omega_{31}$. Taking into account the equations of the planes we can write

$$\begin{aligned} \Omega_{12} &= \{(x_1, x_2, x_3) \in \Omega \mid \alpha_3 x_3 \le \beta_3 x_2,\ x_3 \le \beta_3 x_1\}, \\ \Omega_{23} &= \{(x_1, x_2, x_3) \in \Omega \mid x_3 \ge \beta_3 x_1,\ x_2 \ge \alpha_3 x_1\}, \\ \Omega_{31} &= \{(x_1, x_2, x_3) \in \Omega \mid \alpha_3 x_3 \ge \beta_3 x_2,\ \alpha_3 x_1 \ge x_2\}. \end{aligned}$$

We denote by $\Sigma_i \subset \Pi_i$ the common boundary of Ω_{ij} and Ω_{ki} with $j, k \ne i, j \ne k$. We can check that at each such boundaries Σ_i the vector field is transversal and crosses from Ω_{ki} to Ω_{ij}.

An equation representing Π_1 is $\phi_1(x_1, x_2, x_3) = -\beta_3 x_2 + \alpha_3 x_3 = 0$. The vector grad $\phi_1 = (0, -\beta_3, \alpha_3)$ points from Ω_{12}

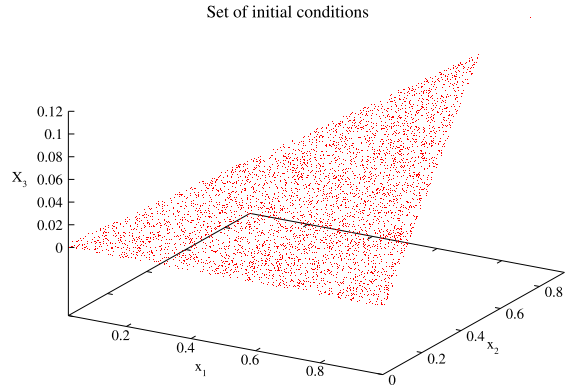

Fig. 8. An example of the set of 5000 initial conditions on Σ_1 whose flow has been integrated numerically to check the non-existence of periodic orbits for $\beta_3 > 0$. The parameter values randomly selected for this particular simulation were $k_{11} = 0.227510$, $k_{12} = 0.140495$, $k_{13} = 0.378144$, $k_{21} = 0.403362$, $k_{32} = 0.432082$, and $\varepsilon = 0.041691$.

to Ω_{31}. We compute the scalar product $F \cdot \operatorname{grad}\phi_1$ and use the conditions that the points belong to Π_1 and Ω_{31}, that is, $x_3 = (\beta_3/\alpha_3)x_2$ and $x_2 \leq \alpha_3 x_1$ respectively. Then, we have

$$\begin{aligned} F \cdot \operatorname{grad}\phi_1 &= -\beta_3(x_2 k_{21} x_1 \theta(x) - \varepsilon x_2) + \alpha_3(x_3 k_{32} x_2 \theta(x) - \varepsilon x_3) \\ &= x_2\theta(x)[-\beta_3 k_{21} x_1 + \alpha_3 k_{32} x_3] \\ &= x_2\theta(x)[-\beta_3 k_{21} x_1 + \beta_3 k_{32} x_2] \\ &= \beta_3 x_2 \theta(x) k_{32}[-\alpha_3 x_1 + x_2] \leq 0. \end{aligned} \tag{12}$$

The inequality is strict except at the boundary of Σ_1. Completely analogous computations check the result for Σ_2 and Σ_3. For Σ_2 we represent ϕ_2 as $\phi_2(x_1, x_2, x_3) = \beta_3 x_1 - x_3 = 0$ and we compute $F \cdot \operatorname{grad}\phi_2$ using $\beta_3 x_1 = x_3$ and $\alpha_3 x_1 < x_2$. For Σ_3 we represent Π_3 as $\phi_3(x_1, x_2, x_3) = -\alpha_3 x_1 + x_2 = 0$ and we compute $F \cdot \operatorname{grad}\phi_3$ using $\alpha_3 x_1 = x_2$ and $x_3 > \beta x_1$.

This suggests that some solutions may turn around the axis generated by v_3 visiting the domains Ω_{12}, Ω_{23} and Ω_{31} in the indicated order and eventually tend to the origin or to the stable fixed point on L_3 (when it exists).

The calculation in (12) shows that Σ_1 is a good Poincaré section for computational purposes. Accordingly, we have used it to compute the Poincaré map, P, numerically and check the non-existence of periodic orbits for a huge set of parameter values and initial conditions. We have chosen random initial conditions on Σ_1 and integrated the system (1)–(3) in forward time. We have checked that all of the trajectories we have considered (i.e., 5000 initial conditions for each of the 100 000 parameter sets, see one instance in Fig. 8), never lead to a periodic orbit. Parameter values were randomly chosen from the set $\{(k_{11}, k_{12}, k_{13}, k_{21}, k_{32}, \varepsilon) \in [10^{-3}, 0.5]\times[10^{-3}, 0.5]\times[10^{-1}, 0.5]\times[10^{-1}, 0.5]\times[10^{-1}, 0.5]\times[10^{-2}, 0.2]\}$. To gain control and reduce the computing time, we additionally implemented several exit conditions to discard initial conditions: either after 2500 time units, or when they reached the basin of attraction of the origin, or the basin of attraction of the line L_3 (see Lemma 1(iii)) or escaped from the simplex Ω, we stopped the computation and took another initial condition. We checked as well that the Poincaré map cannot have periodic orbits of periods 2, 3 or 6, that is, fixed points of P^2, P^3 or P^6.

3. Stochastic spatial dynamics

It has been suggested that mineral surfaces would have played a key role during the emergence of life because the assembly of complex biomolecules in a three-dimensional environment is implausible [37]. In this sense, honeycombed feldspar mineral surfaces could have provided a suitable organized environment for the synthesis of complex molecules, also protecting them from dispersion and hydrolysis. Following these ideas, previous researches have used computational models to investigate the spatial dynamics of hypercycles [38,33,39,40]. In this section we explore the behavior of the hypercycles with short-circuits previously characterized, now considering space in an explicit way. To do so we build stochastic cellular automata (CA) models. To simulate the hypercycle interactions on a surface, we define a state space given by a $L \times L$ lattice, $\mathbf{\Gamma} \in \mathbb{Z}^2$, with periodic boundary conditions (i.e., toroidal space). The automaton has L^2 cells and $\nu + 1$ states, S_n, $n = 1, \ldots, \nu$, being the nth hypercycle member (see Fig. 1(c)), and the other state, S_0, corresponding to empty sites. As in the previous sections, we will focus on hypercycles of size $\nu = 2$ and $\nu = 3$, keeping the catalytic interactions previously analyzed. The CA works as follows. At each generation τ, we asynchronously choose L^2 random cells (this updating procedure ensures that, on average, each cell is updated once per generation). Every time we choose a random cell, say $\mathbf{\Gamma}(x, y)$ (where (x, y) is a spatial coordinate of Γ), we also choose two different random neighbors of $\mathbf{\Gamma}(x, y)$, named $\mathbf{\Gamma}(k, l)$ and $\mathbf{\Gamma}(m, p)$, considering a Moore neighborhood (i.e. 8 nearest cells). If $\mathbf{\Gamma}(x, y)$ is empty nothing will happen. If $\mathbf{\Gamma}(x, y)$ contains a replicator, then we apply the following state-transition rules:

1. **Auto-catalytic replication**: If both cells $\mathbf{\Gamma}(x, y)$ and $\mathbf{\Gamma}(k, l)$ are occupied by S_1, S_1 will replicate with probability $r_{11} \in [0, 1]$ towards $\mathbf{\Gamma}(m, p)$ (if empty). If $\mathbf{\Gamma}(k, l)$ is empty or $\mathbf{\Gamma}(m, p)$ is occupied, nothing will happen. This process is represented by the next reaction:

$$S_1(x, y) + S_1(k, l) + S_0(m, p) + s \xrightarrow{r_{11}} S_1(x, y) + S_1(k, l) + S_1(m, p),$$

hereafter s are some available building blocks (i.e., nucleotides) needed for replication, which are not explicitly considered.

2. **Hetero-catalytic replication**: If the cell $\mathbf{\Gamma}(x, y)$ is occupied by a hypercycle species S_i, and the cell $\mathbf{\Gamma}(k, l)$ is occupied by S_j (where $j = i - 1$ and using the convention that if $i = 1$ then $j = \nu$, thus introducing the cyclic architecture) S_i will replicate with probability $r_{ij} \in [0, 1]$ to $\mathbf{\Gamma}(m, p)$ (provided it is empty). The parameters r_{ij} are the probabilistic version of the constants k_{ij} presented in the mean field equations. This process is represented by the following reactions:

$$S_i(x, y) + S_j(k, l) + S_0(m, p) + s \xrightarrow{r_{ij}} S_i(x, y) + S_j(k, l) + S_i(m, p).$$

The previous reaction for $n = 2$ considers the two-member hypercycle structure. However, for the 3-member hypercycle it does not consider the short-circuit between species S_1 and S_2. Hence, for this larger hypercycle we need to introduce the reaction:

$$S_1(x, y) + S_2(k, l) + S_0(m, p) + s \xrightarrow{r_{12}} S_1(x, y) + S_2(k, l) + S_1(m, p).$$

After replication rule **1** or **2** is applied to $\mathbf{\Gamma}(x, y)$, the replicator in this cell will decay following rule **3**:

3. **Degradation**: The replicator $S_n(x, y)$ will decay with probability $\varepsilon \in [0, 1]$, according to reaction:

$$S_n(x, y) \xrightarrow{\varepsilon} S_0(x, y) + s,$$

with $n = 1, \ldots, \nu$. Here we will also consider equal degradation rates for all the species, as we did for the mean-field model.

After replication and decay rules are applied, we will apply the rule of diffusion, explained below.

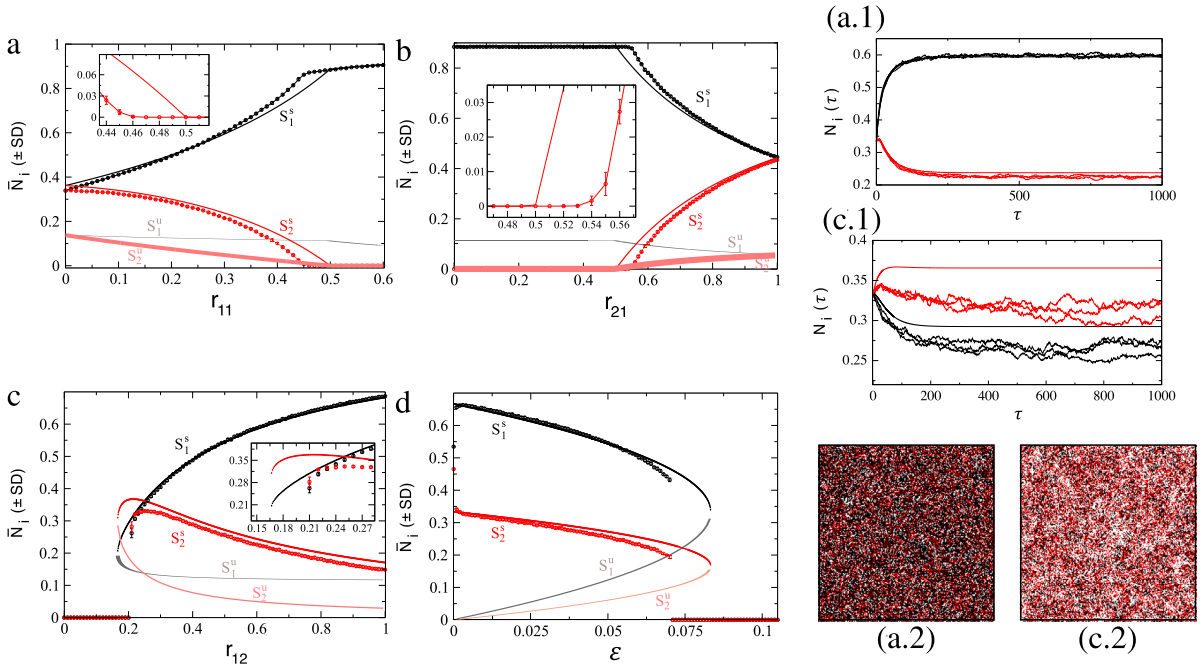

Fig. 9. Spatial and temporal dynamics of the two-member hypercycle with a short-circuit. Populations S_1 and S_2 in all panels are represented, respectively, in black and red. Mean population values ($\bar{N}_i \pm SD$, represented with circles and computed averaging over 10 independent replicas at $\tau = 5000$ time generations) are shown together with the equilibria obtained from the mean field model (solid lines), both the stable (superscript s) and unstable ones (superscript u): (a) tuning r_{11} with $r_{12,21} = 0.5$; (b) tuning r_{21} setting $r_{11} = r_{12} = 0.5$; (c) tuning r_{12} with $r_{11} = 0.25$ and $r_{21} = 0.5$. In (d) we change ε setting $D = 0.25$, $r_{11} = 0.25$, and $r_{12,21} = 0.5$. In (a)-(c) we display the results using $D = 0.25$ and $\varepsilon = 0.05$, using the probabilities r_{ij} as the parameters governing the mean-field model, that is, taking $k_{ij} = r_{ij}$. The insets display an enlarged view of the stable equilibria for S_2 near the transition points. (a.1) Time series using $r_{11} = 0.3$, $r_{12,21} = 0.5$ and $\varepsilon = 0.05$. Here we display, overlapped, 3 runs of the spatial dynamics and the dynamics obtained numerically from the mean field model (solid lines, with $k_{11} = 0.3$, $k_{12,21} = 0.5$, and $\varepsilon = 0.05$). (c.1) Time series with $r_{12} = 0.2$, $r_{11} = 0.25$, $r_{21} = 0.5$, and $\varepsilon = 0.05$. Panels (a.2.) and (c.2) display, respectively, the spatial distribution of replicators at the end of one of the replicates in (a.1) and (c.1), respectively. In all of the simulations we used as initial conditions $N_1(\tau = 0) = N_2(\tau = 0) = 1/3$. (For interpretation of the references to color in this figure legend, the reader is referred to the web version of this article.)

4. **Diffusion**: We choose a random position, say $\mathbf{\Gamma}(q, u)$. If $\mathbf{\Gamma}(q, u)$ contains a replicator, it will diffuse towards a randomly chosen neighbor, $\mathbf{\Gamma}(w, z)$, with probability $D \in [0, 1]$, or remain in the same place with probability $(1 - D)$. Following Ref. [38], if the replicator diffuses, it will interchange the position with the replicator living in the neighboring cell. If the neighbor is empty, it will just move towards the neighbor with probability D. The reaction is

$$S_c(q, u) + S_d(w, z) \xrightarrow{D} S_d(q, u) + S_c(w, z),$$
$$\text{with } c, d = 0, \ldots, \nu.$$

Hereafter, we will denote

$$N_i = \frac{1}{L^2} \sum_{r=1}^{L} \sum_{p=1}^{L} S_i(r, p), \quad \text{with } i = 1, \ldots, \nu,$$

as the normalized population of replicators S_i in $\mathbf{\Gamma}$, N_0 being the normalized number of empty sites. In all of our simulations we will fix $L = 200$, if not otherwise specified. The initial conditions for the two-member hypercycle will be $N_{1,2}(\tau = 0) = 1/3$, while for the three-member hypercycle will be $N_{1,2,3} = 1/4$. All other remaining sites will be empty (i.e., $N_0(\tau = 0) = 1/3$ for the two-member and $N_0(\tau = 0) = 1/4$ three-member hypercycles). Other initial configurations will be used to compute the survival probabilities in the parameter space (see Section 4).

Next, we present the results of this computational model for the two-member hypercycle containing an auto-catalytic species and for the three-member hypercycle containing the previous system, see Fig. 1(a). This will allow us to compare the mean field dynamics with its spatial counterpart, characterizing the critical probability values calculated from the mean field model, and thus unveiling the changes in the survival and extinction patterns introduced by space.

3.1. Spatio-temporal dynamics: the impact of diffusion

Here we investigate the spatio-temporal dynamics for the hypercycle with an inner auto-catalytic short-circuit (Fig. 1(a)). Firstly, we compute the equilibrium population values of species $i = 1, 2$ tuning the CA probabilities. We run several replicates and plot the mean equilibrium population values ($\pm$ standard deviation), $\overline{N}_i(\pm SD)$, for several values of the catalysis and degradation probabilities. In Fig. 9(a) we display the population equilibria tuning the probability of auto-catalytic growth of S_1 averaging, for each probability value, 10 independent replicas after discarding $\tau = 5000$ generations. The populations S_1 and S_2 are shown with black and red circles, respectively. Notice that at increasing r_{11}, the equilibrium populations of S_1 and S_2 increase and decrease, respectively, since the first species undergoes a faster growth. This tendency at increasing r_{11} holds up to a critical value of r_{11} at which the second species of the hypercycle becomes extinct while the population of the first species continues increasing, although more slowly. In these analyses we also plot the equilibrium populations of both replicators obtained numerically from the mean field model previously analyzed using as kinetic constants the same values of the probabilities of the spatial simulations (we also plot the unstable branches of equilibria; we use superscripts s, for stable, and u, for unstable, to distinguish both branches). Notice that the results at increasing r_{11} match the results obtained from the mean-field model (displayed with a solid black (for S_1) and red (S_2) line). The critical value of r_{11} causing the extinction of S_2 populations is slightly lower for the spatial system (see the inset in Fig. 9(a)). For this particular case, S_2 disappears at a lower value of r_{11} compared to the well-mixed system. We note that in panels (a–d) of Fig. 9 we used a diffusion probability of $D = 0.25$. As we will comment on below, diffusion typically

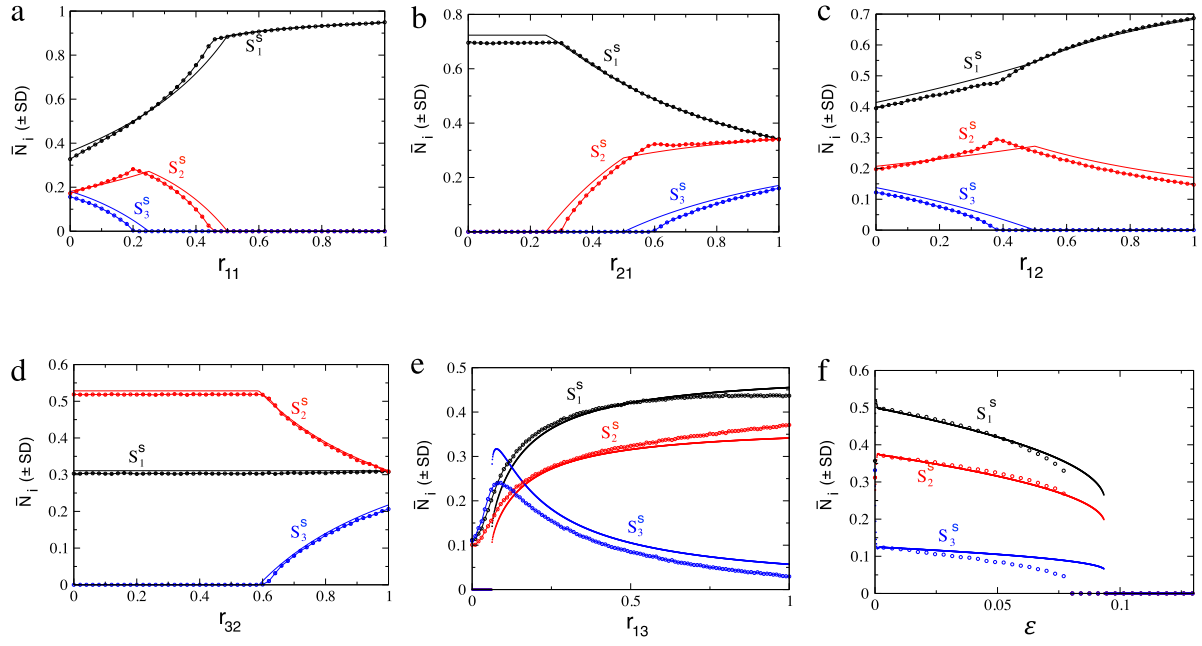

Fig. 10. Dependence of the population equilibria (stable states, $S^s_{1,2,3}$) on the model probabilities for the three-member hypercycle with two short-circuits. Mean population values ($\bar{N}_i \pm SD$, computed averaging over 10 independent replicas at $\tau = 5000$ time generations) for the spatial dynamics, using $D = 0.25$ (circles). In (a) we tune r_{11} setting $r_{12,21,13} = 0.5$ and $r_{32} = 1$. In (b) we change r_{21} setting $r_{11} = 0.25$, $r_{12,13} = 0.5$ and $r_{32} = 1$. In (c) we tune r_{12}, with $r_{11} = 0.25$, $r_{21} = 0.5$, $r_{32} = 1$, and $r_{13} = 0.75$. In (d) we tune r_{32} with $r_{11} = 0.15$, $r_{12,13} = 0.5$, and $r_{21} = 1$. In (e) we change r_{13} with $r_{11} = 0.25$, $r_{12} = 0.5$, $r_{21} = 0.75$, and $r_{32} = 1$. In (a–e) we used $\varepsilon = 0.05$. Finally in (f) we tune ε with $r_{11} = 0.25$, $r_{12,13} = 0.5$, $r_{21} = 0.75$, and $r_{32} = 1$. The solid lines correspond to the predictions of the mean field model using the same values of the probabilities as rate constants e.g., $k_{11} = r_{11}$, $k_{12} = r_{12}$, etc. In all panels populations S_1 and S_2 are represented in black and red, respectively, while S_3 population values are indicated in blue. (For interpretation of the references to color in this figure legend, the reader is referred to the web version of this article.)

affects the critical parameter values causing the transitions in the spatial model (which are homologous to the bifurcations described in the previous sections, and which share the same nature). For instance, the transition of Fig. 9(a) is a continuous and smooth one, corresponding to the transcritical bifurcation.

A smooth transition corresponding also to a transcritical bifurcation is found at decreasing r_{21}. In this case, there exists a critical value of the catalytic aid from species 1 to species 2 that involves the outcompetition of the second hypercycle element by the auto-catalytic one. Here the spatial simulations also reveal a slight difference between the bifurcation value predicted by the mean field model and the one obtained with the CA. Further analyses using r_{12} and ε as control parameters reveal abrupt transitions that correspond to the saddle–node bifurcations predicted by the mean field model. For these two cases, differences between the bifurcation values obtained from the mean field model and the CA simulations are also obtained (the effect of diffusion on the critical parameter values will be analyzed below).

As mentioned above, the dynamics of the CA model matches the dynamics predicted by the mean field model. For example, in Fig. 9(a.1) we display the time dynamics of the two replicators using the same parameter values than in Fig. 9(a) fixing $r_{11} = 0.3$. For this particular parameters combination we plot three runs of the CA model, overlapping the mean field dynamics (solid line). Also, the time dynamics near the transition point in Fig. 9(c) is displayed in Fig. 9(c.1). Here it can be seen that the dynamics predicted by the mean field model matches again the spatial dynamics. This result is general for our spatial model. Finally, in Fig. 9(a.2) and Fig. 9(c.2) we show the spatial patterns of the two replicator species (here also black for S_1 and red for S_2) at the end of one of the simulations displayed in Fig. 9(a.1) and (c.1), respectively, when S_1 and S_2 coexist. The spatial patterns for these runs reveal a well-mixed distribution of the two species. Other simulations in the coexistence scenarios revealed these types of spatial patterns (for the two- and three-member system analyzed below, results not shown).

The dynamics of the three-member hypercycle containing the two-member short-circuit and the auto-catalytic species are displayed in Figs. 10 and 11. Here, similarly to the two-member system, the equilibrium populations are very close to the values predicted by the mean-field model given by Eqs. (1)–(3). This can be seen in panels (a–f) in Fig. 10. The nature of the transitions involved in the extinctions of the different hypercycle members in the spatial model coincide with the bifurcations of the three-member system. For example, the transitions displayed in Fig. 10 are smooth (i.e., transcritical bifurcations) for parameters r_{11} and r_{21} (as we previously described), as well as for r_{12} and r_{32}. Here, the increase of r_{11} beyond the critical value involves the outcompetition of the two- and three-member hypercycle by the auto-catalytic species. However, the increase of r_{21} displays two effects, a first transition involving the survival of the two-member hypercycle and a second one (for a large enough value of r_{21}) that allows the persistence of the three-member system. The parameter r_{32} (i.e., the catalytic aid from species S_2 to S_3) causes, above a critical value, the survival of the three-member system. Below this critical value, the aid of S_2 to S_3 is not large enough to ensure the survival of the whole system. Notice that this parameter has no effect on the population equilibrium of S_1. As we previously did, in all the panels we overlap the equilibrium values for each species predicted by the mean field model (solid lines). As we discussed for the two-member system, there exist small variations in the critical parameter values involved in the transitions.

In Fig. 11(a) we display an example of coexistence of the three hypercycle members. For this particular probabilities combination, species S_3 achieves low population numbers. The spatial patterns of the replicators at $\tau = 0$ (initial random conditions) and $\tau = 5000$ are displayed. Here also, well-mixed (i.e., random-like) spatial patterns are observed at the end of the simulation. Fig. 11(b) displays the spatio-temporal dynamics near the critical value of ε causing the extinction of all the species. Here, while the dynamics for the mean field model under these parameters combination

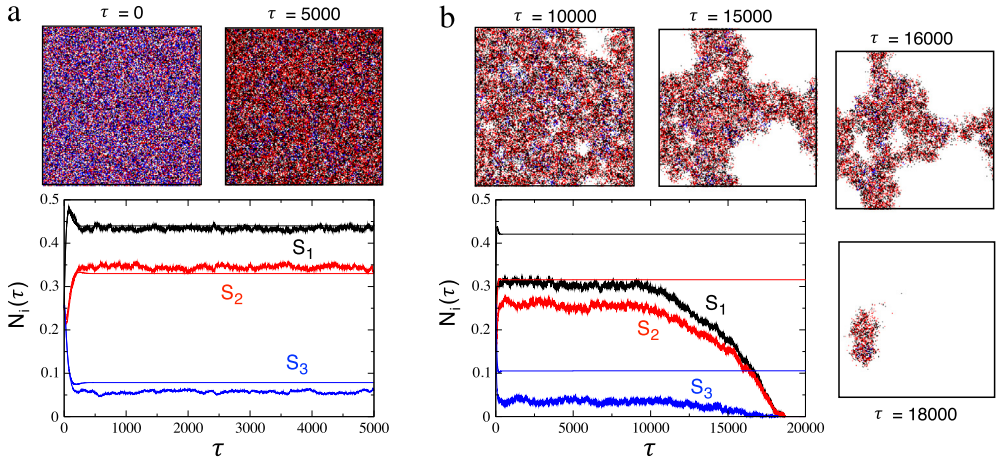

Fig. 11. Spatio-temporal dynamics for $n = 3$ hypercycles with short-circuits (here also: S_1 (black), S_2 (red), and S_3 (blue)). (a) Coexistence scenario with: $r_{11} = 0.25$, $r_{21} = 0.75$, $r_{12} = 0.5$, $r_{13} = 0.7$, $r_{32} = 1$, $D = 0.25$, and $\varepsilon = 0.05$. (b) Coextinction of all hypercycle members near a saddle–node bifurcation using the same parameters as in (a) except for: $r_{13} = 0.5$, and $\varepsilon = 0.0792$. The solid trajectories are the predictions of the mean field model using the probabilities values of the CA as constants. Notice that in the extinction the system undergoes a long transitory plateau before a rapid collapse. Here, noise drives the system to undergo the so-called saddle-remnant (ghost) effect that arises in the deterministic system after a saddle–node bifurcation (see e.g., [41,42]). For each of the simulations we display the spatial patterns at different times. (For interpretation of the references to color in this figure legend, the reader is referred to the web version of this article.)

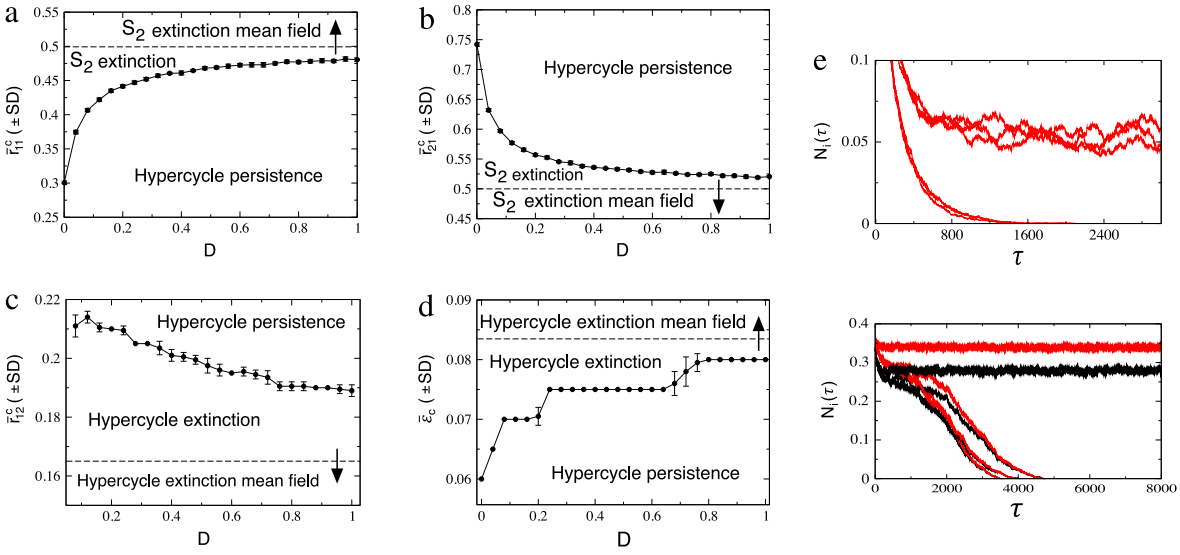

Fig. 12. (a–d) Critical parameter values causing the transitions for the two-member hypercycle with the short-circuit identified in Fig. 9(a–d), computed setting $\tau = 2 \times 10^4$, for different diffusion probabilities. Each data point is the mean value ($\pm SD$) of the critical parameter ($\bar{r}^c_{11}$ in (a), $\bar{r}^c_{21}$ in (b), $\bar{r}^c_{12}$ in (c), and $\bar{\varepsilon}_c$ in (d)) averaged over 10 independent runs. The dashed lines indicate the transition values predicted by the mean field model, using the probabilities as parameters. (e) Dynamics for different diffusion probabilities driving to extinction or survival scenarios: (upper) we set $r_{11} = 0.45$, $r_{12,21} = 0.5$, $\varepsilon = 0.05$, with $D = 0.05$ (S_2 extinction) and $D = 0.8$ (hypercycle survival), here we only plot the population of S_2 (red). (lower) Simulations using $r_{11} = 0.25$, $r_{12} = 0.2$, $r_{21} = 0.5$, with $D = 0.3$ (hypercycle extinction) and $D = 0.9$ (hypercycle survival), here we display the population dynamics for S_1 (black) and S_2 (red). In each panel in (e) we display 3 different runs for each value of diffusion. (For interpretation of the references to color in this figure legend, the reader is referred to the web version of this article.)

does not involve the extinction of the whole hypercycle (ε is below its critical value causing the saddle–node bifurcation), the spatial dynamics involves the extinction. Interestingly, the time trajectory, which achieves extinction at $\tau \approx 19\,000$ generations, undergoes a long and flat plateau before collapsing. This dynamical effect, which has been described for two-member hypercycles (for both mean field and spatial stochastic dynamics [41]) is due to the transient behavior near a saddle–node bifurcation, which is extremely long causing the so-called delayed transition [38]. The asymptotic state for this scenario is an absorbing state where the full hypercycle becomes extinct, as reported in [41]. The simulation displayed in Fig. 11(b) falls in the extinction regime, where the flat plateau preceding extinction can be clearly seen.

Up to now, we have discussed the impact and the transitions tied to the auto-catalytic and hetero-catalytic probabilities among replicators, having evidences that diffusion slightly changes the values of these parameters causing the bifurcations when compared to the values predicted by the mean field models. In order to analyze how diffusion affects these transition values, we computed the critical probability values causing the transitions in the populations at increasing values of the diffusion probability D. For the two-member system we display the results in Fig. 12. For each value of D we ran 10 simulations (replicas) during $\tau = 2 \times 10^4$ generations for several values of the investigated probabilities (e.g., r_{11} in Fig. 12(a)). From all these replicas we computed the mean probability value causing a change of behavior. For example, separating the survival from the extinction of S_2. Then we plotted the mean critical values against probability D. Fig. 12(a) displays the results for the mean critical probability of auto-catalytic growth, $\bar{r}^c_{11}(\pm SD)$, causing the transition towards S_2 extinction. As expected, for maximum values of D, the critical value approaches the one predicted by the mean field model (this result

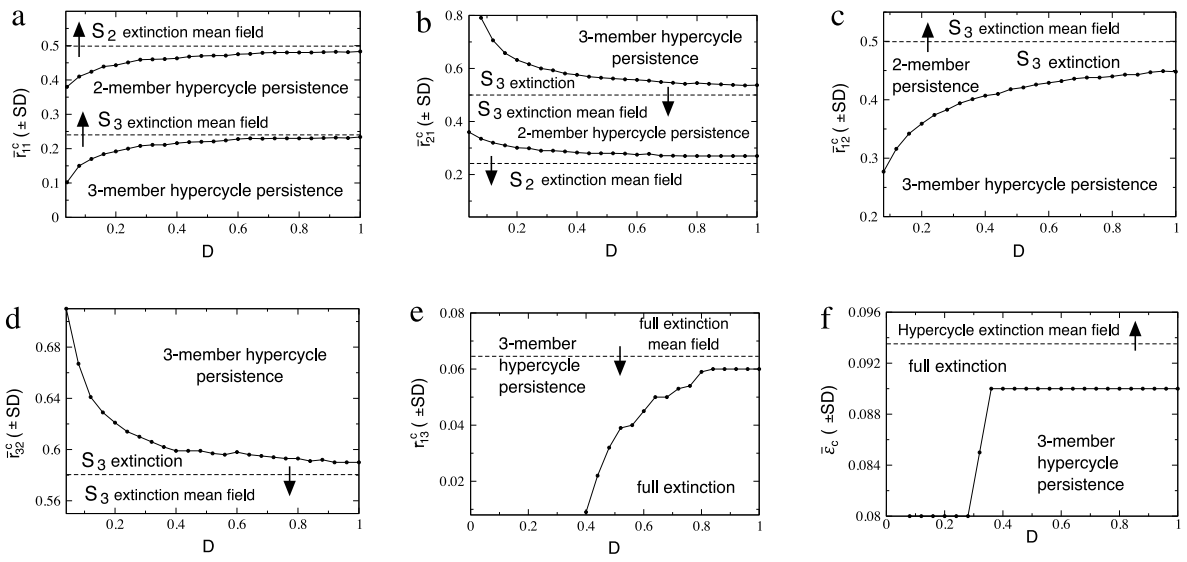

Fig. 13. Critical parameter values causing the different transitions displayed in Fig. 10 tuning the diffusion probability. Here each data point is the mean value ($\pm SD$) of the critical parameters averaged over 10 independent runs (at $\tau = 2 \times 10^4$ generations). Here the dashed lines indicate the transition values predicted by the mean field model. We specifically computed (a) $\bar{r}^c_{11}$, (b) $\bar{r}^c_{21}$, (c) $\bar{r}^c_{12}$, (d) $\bar{r}^c_{32}$, (e) $\bar{r}^c_{13}$, and (f) $\bar{\varepsilon}_c$. The parameter values used for each panel are the same as in Fig. 10.

is observed in all of our analyses, see Figs. 12 and 13). Low values of D promote (under the analyzed parameters combination) the extinction of S_2, while increasing D values make the value of $\bar{r}^c_{11}$ larger. This indicates that mixing favors the survival of the two-member hypercycle. The effect of D in the critical value of r_{21} is similar to the previous case. The increase of the catalytic aid of the first replicator to the second one promotes the survival of the whole hypercycle. The changes in the critical probabilities for r_{12} and ε are displayed in Fig. 12(c) and (d), respectively. In Fig. 12(e) we display several trajectories for which changes in D involve a qualitative change in the dynamics i.e., survival or extinction depending on diffusion.

The same analyses have been carried out for the three-member system. The results can be found in Fig. 13. Here we must notice that several bifurcations can be found tuning a single parameter. For instance, as shown in Fig. 10(a), the increase of r_{11} involves a first bifurcation that causes the extinction of S_3 and then there exists a second critical value causing S_2 extinction. Both transitions are governed by transcritical bifurcations. To account for these different values, different probability values have been sampled to find their critical values. For instance, Fig. 13(a) displays the mean critical values of r_{11} that involve the survival of the whole three-member system, of the two-member hypercycle, and of the auto-catalytic replicator. Diffusion, for both transitions, is shown to increase the values of r^c_{11} at which the transition takes place, favoring the persistence of all replicators since a higher value of r^c_{11} is needed for S_1 to outcompete the hypercycles. The critical values of the other parameters as a function of diffusion are displayed in Fig. 13. We notice that in all of the panels displayed in Figs. 12 and 13, we also plot (using a dashed line) the bifurcation values predicted by the mean field model.

4. Hypercycle persistence in parameter space

In our previous analyses we have focused on the dynamics and the transitions obtained from both mean field and stochastic spatial models for the hypercycles with the short-circuits. However, it is also interesting to characterize how probable it is to find all of the characterized scenarios in the parameter spaces of both systems. For instance, how probable is the coexistence of all the hypercycle species or how probable is the persistence of only the first autoacatalytic replicator, thus obtaining a simpler system with a lower potential information. In this section we will estimate the likelihood of survival of each of the replicators in the parameter space of the two model approaches: mean field and spatial stochastic models. To do so, we built a Monte Carlo (MC) algorithm, which works as follows for the two modeling approaches. At each MC iteration, M, we randomly select the model parameters (probabilities in the CA) from a uniform distribution. For the two-member system we select $\{k_{11}, k_{21}, k_{12}\} \in \mathcal{U}(0, 1)$ for the mean field model (and $\{r_{11}, r_{21}, r_{12}, D\} \in \mathcal{U}(0, 1)$ for the CA). For the three-member hypercycle, we proceed in a similar way, selecting randomly the parameters $\{k_{11}, k_{21}, k_{12}, k_{32}, k_{13}\} \in \mathcal{U}(0, 1)$ for the mean field model (and $\{r_{11}, r_{21}, r_{12}, r_{32}, r_{13}, D\} \in \mathcal{U}(0, 1)$ for the CA). For each selected combination of random parameters we integrate numerically the mean field model (for which we study to final values of time $t = 2.5 \times 10^4$ and $t = 5 \times 10^4$) or run simulations for the CA (with $\tau = 10^4$). At these times the population of each hypercycle member is evaluated.

For the two-member hypercycle with the short-circuit two possible scenarios (predicted by the mean field model) are possible: only-survival of S_1 given by scenario (A), and scenario (B) where the hypercycle replicators S_1 and S_2 coexist. Similarly, scenarios (A) and (B) are also found for the three-member hypercycle. For this case, another scenario is possible: scenario (C) where the three replicator species survive. For the mean field model, the survival of species i is considered when $x_i > 10^{-5}$ (with $i = 1, 2, 3$) and thus extinction is assumed with $x_i \leq 10^{-5}$. For the CA model, since replicators only replicate catalytically, we assume survival when $S_i \geq 2$ and extinction if $S_i \leq 1$. As a first approach (case (i) in Table 2) we use the same initial population values: $x_{1,2}(0) = 1/3$ (two-member hypercycle) and $x_{1,2,3}(0) = 1/4$ (three-member system) in the mean field model; and $N_{1,2}(\tau = 0) = 1/3$ and $N_{1,2,3}(\tau = 0) = 1/4$ for the CA model. However, different initial configurations will be also analyzed (see below and Table 2).

First, we display those regions in the probabilities space of the CA where each scenario is found by means of two-dimensional projections (Fig. 14). For the two-member hypercycle we display the spaces (r_{11}, r_{21}) and (r_{21}, D). The different scenarios in the probabilities space (r_{11}, r_{21}) are clearly separated, with scenario (A) dominating at increasing values of r_{11}. From the MC simulations we can estimate the survival probability Π_S of the replicators for each of the scenarios above. Such a probability is computed as:

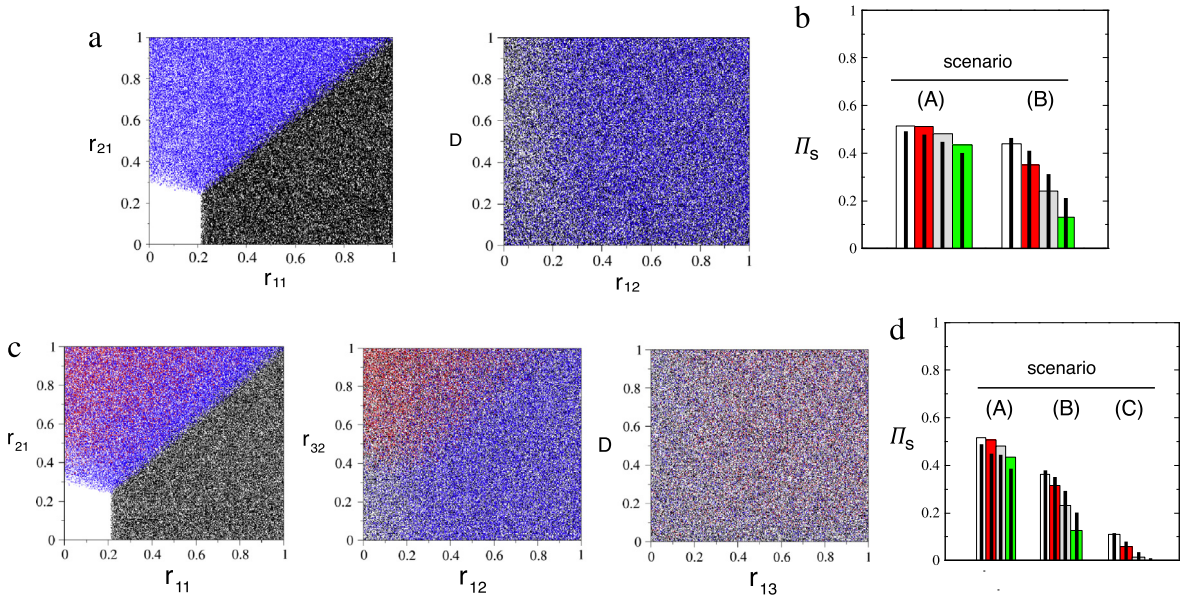

Fig. 14. Monte Carlo (MC) sampling in the parameter spaces setting $\varepsilon = 0.05$, $\tau = 10^4$, and $L = 100$. (a) Projections on (r_{11}, r_{21}) and (r_{12}, D), for the spatially-extended two-membered hypercycle. Black dots indicate those regions in each parameter space with only survival of S_1 (scenario (A)) while blue dots indicate persistence of the two species (scenario (B)). (b) Computation of the survival probability Π_s for the scenarios (A) and (B) from the MC sampling for $\varepsilon = 0.025$ (white bars); $\varepsilon = 0.05$ (red bars); $\varepsilon = 0.075$ (gray bars); and $\varepsilon = 0.1$ (green bars). The thick lines inside the bars of the histogram (also represented in (d)) are the values of Π_S obtained from the MC sampling of the mean field model. (c) Same analysis for the three-membered hypercycle with the short-circuits. As before, we plot those pairs of values giving place to scenario (A) (black dots); and scenario (B) (blue dots). Here another scenario given by the survival of the three-member hypercycle is possible (scenario (C), red dots). The projections are displayed in the probability spaces (a) (r_{11}, r_{21}), (b) (r_{12}, r_{32}), and (c) (r_{13}, D). (d) Survival probability (Π_S) for each of the three scenarios (A), (B), and (C) computed as in (b). The MC algorithm was run over $M = 2 \times 10^5$ iterations for both mean field and CA simulations. In all the analyses we used $N_{1,2}(0) = 1/3$ for $n = 2$; $N_{1,2,3}(0) = 1/4$ for $n = 3$ as initial populations for the CA. For the mean field we set $x_{1,2}(0) = 1/3$ for $n = 2$; $x_{1,2,3}(0) = 1/4$ for $n = 3$ as initial conditions (case (i) in Table 2). (For interpretation of the references to color in this figure legend, the reader is referred to the web version of this article.)

Table 2

Survival probabilities (Π_S) computed with the Monte Carlo (MC) algorithm (from $M = 2 \times 10^5$ iterations). We use four different values of degradation: $\varepsilon = 0.025, 0.05, 0.075, 0.1$, and three different initial conditions (cases (i–iii)). For the mean field ($x_i(0)$) and the CA model ($N_i(0)$): case (i) $s_i(0) = 1/3$ for $n = 2$; $s_i(0) = 1/4$ for $n = 3$. Case (ii) $s_1(0) = 0.6$ and $s_2(0) = 0.1$ for $n = 2$; $s_1(0) = 0.6$ and $s_{2,3}(0) = 0.1$ for $n = 3$. Case (iii) $s_1(0) = 0.1$ and $s_2(0) = 0.6$ for $n = 2$; $s_{1,2}(0) = 0.1$, and $s_3(0) = 0.6$ for $n = 3$, with $s_i(0) \in \{x_i(0), N_i(0)\}$. In the mean field we consider survival of replicator i if $x_i > 10^{-5}$ and extinction if $x_i \leq 10^{-5}$ at $t = 25\,000$ (the values inside the parentheses display the same simulations using $t = 5 \times 10^4$). For the CA we use $L = 100$, considering $S_i > 1$ (survival) and $S_i \leq 1$ (extinction) at $\tau = 10^4$.

Hypercycle	Scenario	Π_S, mean field dynamics				Π_S, spatial dynamics			
		$\varepsilon = .025$	$\varepsilon = .05$	$\varepsilon = .075$	$\varepsilon = .1$	$\varepsilon = .025$	$\varepsilon = .05$	$\varepsilon = .075$	$\varepsilon = .1$
$n = 2$	(A)	0.4891 (0.4925)	0.4758 (0.4768)	0.4475 (0.4460)	0.4001 (0.4017)	0.5118	0.5069	0.4821	0.4359
Case (i)	(B)	0.4684 (0.4655)	0.4017 (0.3993)	0.3133 (0.3116)	0.2129 (0.2128)	0.4426	0.3527	0.2410	0.1284
$n = 2$	(A)	0.4893 (0.4943)	0.4797 (0.4787)	0.4550 (0.4549)	0.4174 (0.4192)	0.5114	0.5082	0.4841	0.4428
Case (ii)	(B)	0.4683 (0.4633)	0.3994 (0.3988)	0.3138 (0.3114)	0.2153 (0.2152)	0.4432	0.3517	0.2427	0.1298
$n = 2$	(A)	0.4848 (0.4887)	0.4416 (0.4426)	0.3494 (0.3476)	0.2450 (0.2448)	0.5108	0.5005	0.4604	0.3938
Case (iii)	(B)	0.4655 (0.4622)	0.3834 (0.3815)	0.2751 (0.2768)	0.1627 (0.1611)	0.4414	0.3482	0.2302	0.1138
$n = 3$	(A)	0.4880 (0.4927)	0.4751 (0.4773)	0.4444 (0.4427)	0.3876 (0.3899)	0.5123	0.5076	0.4792	0.4325
Case (i)	(B)	0.3732 (0.3694)	0.3421 (0.3409)	0.2843 (0.2846)	0.1944 (0.1938)	0.3556	0.3117	0.2324	0.1261
	(C)	0.1147 (0.1143)	0.0815 (0.0805)	0.0329 (0.0332)	0.0041 (0.0043)	0.1045	0.0566	0.0098	1.5×10^{-5}
$n = 3$	(A)	0.4931 (0.4923)	0.4781 (0.4793)	0.4562 (0.4558)	0.4199 (0.4184)	0.5134	0.5075	0.4839	0.4409
Case (ii)	(B)	0.3701 (0.3716)	0.3438 (0.3421)	0.2862 (0.2878)	0.2074 (0.2095)	0.3597	0.3155	0.2333	0.1317
	(C)	0.1124 (0.1116)	0.0777 (0.0779)	0.0314 (0.0315)	0.0038 (0.0041)	0.0994	0.0539	0.0091	1.5×10^{-5}
$n = 3$	(A)	0.4898 (0.4900)	0.4537 (0.4542)	0.3632 (0.3638)	0.2373 (0.1779)	0.5109	0.5011	0.4653	0.4005
Case (iii)	(B)	0.3678 (0.3683)	0.3078 (0.3088)	0.1946 (0.1953)	0.0887 (0.0851)	0.3573	0.3047	0.2007	0.0907
	(C)	0.1117 (0.1113)	0.0723 (0.0714)	0.0231 (0.0234)	0.0015 (0.0017)	0.1015	0.0508	0.0068	5×10^{-7}

$\Pi_S = N_S/M$, where N_S is the number of probabilities (parameters) combinations fulfilling the survival condition of each scenario, and M is the number of MC iterations (we use $M = 2 \times 10^5$). We notice that larger values of M gave qualitatively similar results (results not shown).

The results for the two-member hypercycle with the auto-catalytic replicator are found in Fig. 14(b). Notice that the probability to find scenario (A) is larger than the one for scenario (B). This result is accentuated for large values of the degradation rate, ε. Here, we also computed these probabilities numerically from the mean field model, and the results have been overlapped to the histograms with a black vertical line for each scenario and value of ε. The values of Π_S are similar between the mean field and the CA models. The same computations have been carried out for the three-member hypercycle. Here, as shown in the projections of Fig. 14(c) as well as in the histogram of Fig. 14(d), scenario (c) becomes less probable in the parameter space. This actually means that the likelihood of persistence for the three-member hypercycle in the parameter space is low. This result becomes clear in the histogram. For low values of ε (i.e., $\varepsilon = 0.025$), the survival probabilities of the first species are $\Pi_S \approx 0.5$. For the same degradation rates, the probability to find the two-member hypercycle is of $\Pi_S \approx 0.37$, while for the three-member hypercycle this probability becomes $\Pi_S \approx 0.1$. These differences

become stronger at increasing degradation rates. For instance, $\Pi_S \approx 0.45$ for scenario (A), $\Pi_S \approx 0.1$ for scenario (B), and $\Pi_S \approx 10^{-5}$ for scenario (C), when $\varepsilon = 0.1$. The values of Π_S for all the other scenarios and degradation rates are shown in Table 2 (case (i)).

The previous results have been computed using a given initial configuration of replicators (or initial conditions). Specifically, starting with equal populations for each of the replicator species (case (i)). Since in Section 2 we characterized saddle–node bifurcations, there will exist (for some parameter values) scenarios of bistability. It means that depending on the initial conditions, different asymptotic states may be achieved. Hence, we repeated the analyses for the mean field and the CA models considering two different cases: case (ii): $s_1(0) = 0.6$ and $s_2(0) = 0.1$ for $n = 2$; $s_1(0) = 0.6$ and $s_{2,3}(0) = 0.1$ for $n = 3$. Case (iii): $s_1(0) = 0.1$ and $s_2(0) = 0.6$ for $n = 2$; $s_{1,2}(0) = 0.1$, and $s_3(0) = 0.6$ for $n = 3$, with $s_i(0) \in \{x_i(0), N_i(0)\}$. The results are also displayed in Table 2. Similar results to case (i) have been obtained. However, Π_S for case (iii) diminishes for the mean field model, especially for $\varepsilon = 0.075$ and $\varepsilon = 0.1$, where the survival probabilities become smaller when compared to the other two cases.

5. Conclusions

The nature of the first self-replicating systems on Earth and how they might have grown in complexity remain an open question. However, compelling evidences indicate that ribozymes might be good candidates for primordial replicative systems [1,24,23]. Ribozymes are catalytic RNA molecules that can be both functional and message carriers. In this sense, ribozymes could have been the building blocks of the so-called hypercycles. Pointing in this direction, recent experimental findings [23] revealed that variants of bacteria ribozymes could assemble to form cooperative cycles, being able to outcompete smaller auto-catalytic cycles. Hypercycles have been widely investigated since Eigen and Schuster proposed them. Hypercycles would integrate and ensure the coexistence of several, distinct templates by means of cooperation. Eigen and Schuster argued that such a system might be able to store further information by integrating several templates, each of them below the critical length imposed by the error threshold [10]. Hypercycles were early criticized mainly because catalytic parasites and short-circuits could impair their growth. While the impact of parasites has been largely investigated [33,35,34], the dynamics and transitions caused by short-circuits remain largely unexplored.

In this article we provide a full description of the dynamics for two small hypercycles containing inner catalytic cycles using mean field and stochastic spatial simulations. The first system is a two-member hypercycle in which one of the replicators is auto-catalytic, thus being the smallest hypercycle with a short-circuit. Then, we extend this system by adding another species to the two-member hypercycle thus closing a three-member hypercycle with two short-circuits inside. We study these particular architectures since we are interested in a possible system that might have evolved from the two-member hypercycle, in which a new mutant species could have been synthesized increasing the size of the hypercycle while keeping the previous structure. Although we are not explicitly modeling this growth, we are interested in analyzing the changes in the dynamics and the bifurcations found in this larger system, as well as in the dynamics of the smaller one. The mean field models allow us to provide a detailed description of the nature of the bifurcations involving the reduction of the hypercycles and the dominance of the inner short-circuits. Moreover, the spatial simulations reveal that the dynamics is very similar to the one predicted by the mean field models, especially at maximum diffusion probabilities. The mean field model also allowed us to discard the presence of periodic orbits for both two- and three-member systems. Both mean field and spatial models reveal scenarios where all the hypercycle species coexist in a stable manner, being the hypercycle able to coexist with the members establishing shorter, inner cycles. Although this coexistence scenario drastically reduces at increasing degradation rates.

It is known that oscillating hypercycles (hypercycles with $n > 4$ members) typically form self-organized spatial patterns. For instance, spiral waves [33,35] or clusters [43]. Such spatial patterns have been suggested to be crucial for the survival of the hypercycle under the presence of parasites. Moreover, the presence of spiral waves also ensured the exclusive coexistence between hypercycles and inner catalytic cycles [35]. As mentioned, our results indicate that no oscillations are found in the mean field models, suggesting that no oscillatory behavior may be found in the spatial simulations. Indeed, the spatial patterns obtained in our simulations are given by well-mixed (random-like) patterns. Our results suggest that without self-structuring, small hypercycles are very sensitive to the short-circuits, especially at increasing degradation rates. Following our results and [35], it seems that a minimum number of hypercycle species would be required prior to the emergence of the short-circuits to ensure the formation of large-scale spatial patterns allowing a stable coexistence with the short-circuits in a stable manner. As mentioned, however, under appropriate parametric conditions (especially at low degradation rates), the hypercycles are able to persist with the short-circuits. These results have been found in both the mean field and spatial models.

Finally, as stated by Kauffman [1]: "The essential feature of auto-catalysis is independent of its precise biochemical definition. Therefore, study on auto-catalysis would also be applicable to several areas including ecosystems, immune system, and neural and social networks". Hence, our results can be useful for other catalytic systems beyond the origins-of-life molecular hypercycles, in which inner cycles may arise. For instance, our results can help to build synthetic cooperative systems containing short-circuits. In this sense, recent articles have reported the experimental building of synthetic cooperative populations in bacteria [44] and yeast [45] populations.

Acknowledgments

We want to thank the members of the Complex Systems Lab for their comments, as well as José Antonio Darós for suggestions. We acknowledge the use of the UPC Dynamical Systems Group cluster for research computing (see http://dynamicalsystems.upc.edu/en/computing). This work has been partially funded by the Botín Foundation, by Banco Santander through its Santander Universities Global Division (JS); by the CERCA Programme of the Generalitat de Catalunya (Centre de Recerca Matemàtica (CRM) to JS); the Spanish grants MINECO MTM2013-41168-P (EF), MTM2015-71509-C2-2-R (AG) and MTM2015-65715-P (JTL); the Catalan grants AGAUR 2014SGR-1145 (EF) and 2014SGR-504 (AG, JTL); the grant 14-41-00044 of RSF at the Lobachevsky University of Nizhny Novgorod (Russia) (JTL); and the European Marie Curie Action FP7-PEOPLE-2012-IRSES: BREUDS (JTL). JTL also thanks the CRM for its hospitality during the last period of writing of this work. The research leading to these results has received funding from "la Caixa" Foundation.

Appendix

A.1. Proof of Proposition 2

To ease the reading the proof has been divided into three cases.

A.1.1. Case I: fixed points of the form $(x_1, 0, 0)$

The differential $DF(x_1, 0, 0)$ is given by the following triangular matrix

$$\begin{pmatrix} k_{11}\left(2x_1(1-x_1)-x_1^2\right)-\varepsilon & k_{12}x_1(1-x_1)-k_{11}x_1^2 & k_{13}x_1(1-x_1)-k_{11}x_1^2 \\ 0 & k_{21}x_1(1-x_1)-\varepsilon & 0 \\ 0 & 0 & -\varepsilon \end{pmatrix},$$

whose eigenvalues are

$$\lambda_1 = k_{11}\left(2x_1(1-x_1)-x_1^2\right)-\varepsilon,$$
$$\lambda_2 = k_{21}x_1(1-x_1)-\varepsilon, \qquad \lambda_3 = -\varepsilon.$$

- Regarding points $P^{\pm}$, for simplicity, let us denote, p_1 to indicate the first component $p_1^{\pm}$ of $P^{\pm}$. From Proposition 1, p_1 satisfies $p_1^2 - p_1 + \varepsilon/k_{11} = 0$. So, the first eigenvalue satisfies

$$\lambda_1 = k_{11}\left(\left(-p_1^2+p_1-\frac{\varepsilon}{k_{11}}\right)+\left(-2p_1^2+p_1\right)\right) = 2k_{11}p_1\left(\frac{1}{2}-p_1\right).$$

  Using that $p_1^+ > 1/2$ and $p_1^- < 1/2$ it is clear that $\lambda_1^+ < 0$ and $\lambda_1^- > 0$. On the other hand, since $(1-p_1^{\pm})p_1^{\pm} = \varepsilon/k_{11}$ we have

$$\lambda_2^{\pm} = k_{21}p_1(1-p_1)-\varepsilon = k_{21}\frac{\varepsilon}{k_{11}}-\varepsilon = \frac{k_{21}-k_{11}}{k_{11}}\varepsilon,$$

  whose sign depends on the difference $k_{21}-k_{11}$. The eigenvalues $\lambda_3^{\pm} = -\varepsilon$ are always negative.
- At the point $P^0 = (1/2, 0, 0)$ we have $\varepsilon = \varepsilon_1 = k_{11}/4$ and $x_1 = 1/2$. Thus, the previous formulae read

$$\lambda_1^0 = 0, \qquad \lambda_2^0 = \frac{k_{21}-k_{11}}{4}, \qquad \lambda_3^0 = -\varepsilon_1 < 0.$$

A.1.2. Case II: fixed points of the form $(x_1, x_2, 0)$

We remind that $Q^{\pm,0} = (q_1^{\pm,0}, \alpha_2 q_1^{\pm,0}, 0)$ and let us introduce $\theta^{\pm,0} = (1 - q_1^{\pm,0} - \alpha_2 q_1^{\pm,0}) = (1-\mu_2 q_1^{\pm,0})$, and $\Sigma^{\pm,0} = k_{11}q_1^{\pm,0} + k_{12}\alpha_2 q_1^{\pm,0}$. The condition of $Q^{\pm,0}$ being equilibrium points gives $\Sigma^{\pm,0}\theta^{\pm,0} = \varepsilon$, $k_{21}q_1^{\pm,0}\theta^{\pm,0} = \varepsilon$. To simplify the notation we will not write the superscripts $(\pm, 0)$. Using the previous relations and notation we have

$$DF(Q) = \begin{pmatrix} k_{11}q_1\theta - k_{21}q_1^2 & k_{12}q_1\theta - k_{21}q_1^2 & k_{13}q_1\theta - k_{21}q_1^2 \\ k_{21}\alpha_2 q_1(\theta - q_1) & -k_{21}\alpha_2 q_1^2 & -k_{21}\alpha_2 q_1^2\theta \\ 0 & 0 & k_{32}\alpha_2 q_1\theta - \varepsilon \end{pmatrix}.$$

From the block structure of $DF(Q)$ one gets that

$$\lambda_1 = k_{32}\alpha_2 q\theta - \varepsilon = \left(\frac{k_{32}}{k_{21}}\cdot\frac{k_{21}-k_{11}}{k_{12}}-1\right)\varepsilon = \frac{k_{13}}{k_{12}}\frac{\beta_3}{\alpha_3}\varepsilon$$

is an eigenvalue. We know that $Q^{\pm,0}$ are located on the line L_2. Since it is an invariant line, $v_2 = (1, \alpha_2, 0)$ is an eigenvector of $DF(Q^{\pm,0})$. Computing $DF(Q^{\pm,0})v_2$ will provide the corresponding eigenvalue. Indeed, $DF(Q)v_1 = (\varepsilon - k_{21}\mu_2 q^2)v_1$, so it follows that

$$\lambda_2 = \varepsilon - k_{21}\mu_2 q^2$$

is another eigenvalue. Finally, from the trace of $DF(Q)$ we get the third eigenvalue,

$$\lambda_3 = \operatorname{tr} DF(Q) - \lambda_1 - \lambda_2 = k_{11}q\theta - k_{21}q(1-\mu_2 q) = -\alpha_2\varepsilon.$$

Observe that the sign of the eigenvalues λ_1 and λ_3 does not depend on ε but only on the values of the parameters k_{ij}. Precisely, we have $\operatorname{sign}(\lambda_1^{\pm,0}) = \operatorname{sign}(\beta_3)$ and $\lambda_3^{\pm,0} < 0$ since $k_{11} < k_{21}$. However, the sign of λ_2 is different for λ_2^+, λ_2^- and λ_2^0. Let us show this by expressing λ_2 in a more suitable form. Thus,

$$\begin{aligned}\lambda_2^{\pm} &= \varepsilon - k_{21}\mu_2\left(q_1^{\pm}\right)^2 = \varepsilon - \frac{k_{21}}{4\mu_2}\left(1\pm\sqrt{1-\frac{\varepsilon}{\varepsilon_2}}\right)^2 \\ &= \varepsilon - \varepsilon_2\left(2-\frac{\varepsilon}{\varepsilon_2}\pm 2\sqrt{1-\frac{\varepsilon}{\varepsilon_2}}\right) \\ &= 2\left(-(\varepsilon_2-\varepsilon)\mp\sqrt{\varepsilon_2}\sqrt{\varepsilon_2-\varepsilon}\right) \\ &= -2\sqrt{\varepsilon_2-\varepsilon}\left(\sqrt{\varepsilon_2-\varepsilon}\pm\sqrt{\varepsilon_2}\right),\end{aligned}$$

so $\lambda_2^+ < 0$, $\lambda_2^- > 0$, and $\lambda_2^0 = 0$. If $\varepsilon = \varepsilon_2$, the other two eigenvalues are given by $\lambda_1^0 = \frac{k_{13}}{k_{12}}\frac{\beta_3}{\alpha_3}\varepsilon_2$, $\lambda_3^0 = -\alpha_2\varepsilon_2$.

In the particular case $k_{11} = k_{21}$ the points $Q^{\pm,0}$ coincide with the points $P^{\pm,0}$.

A.1.3. Case III: fixed points of the form (x_1, x_2, x_3)

Assuming now that $x_1x_2x_3 \neq 0$ leads, in (1)–(3), to $x_2 = k_{21}/k_{32}x_1 = \alpha_3 x_1$. Thus, the differential matrix becomes

$$DF(R^{\pm,0}) = \begin{pmatrix} \frac{k_{11}}{k_{21}}\varepsilon - k_{21}r_1^2 & \frac{k_{12}}{k_{21}}\varepsilon - k_{21}r_1^2 & \frac{k_{13}}{k_{21}}\varepsilon - k_{21}r_1^2 \\ \alpha_3(\varepsilon - k_{21}r_1^2) & -\frac{k_{21}^2}{k_{32}}r_1^2 & -\frac{k_{21}^2}{k_{32}}r_1^2 \\ -k_{21}\beta_3 r_1^2 & \beta_3\left(\frac{k_{32}}{k_{21}}\varepsilon - k_{21}r_1^2\right) & -k_{21}\beta_3 r_1^2 \end{pmatrix},$$

where r_i denotes $r_i^{\pm,0}$, $i = 1, 2, 3$, each of the components of the points $R^{\pm,0}$ and it has been used that $\varepsilon/\theta = k_{21}r_1 = k_{32}r_2$ and $r_2 = \alpha_3 r_1$, $r_3 = \beta_3 r_1$. The computation of its eigenvalues can be carried out using that the invariant line to where they belong provides the eigenvector $(1, \alpha_3, \beta_3)$ and, consequently, its associated eigenvalue. The other two eigenvalues are obtained using the determinant and the trace of the matrix. Like in the previous cases, we denote by $(\lambda_1^{\pm}, \lambda_2^{\pm}, \lambda_3^{\pm})$ and $(\lambda_1^0, \lambda_2^0, \lambda_3^0)$ the associated eigenvalues to the equilibrium points $R^{\pm}$, R^0, respectively.

We start dealing with $R^{\pm}$. A first eigenvalue $\lambda_1^{\pm}$ is given by the expression

$$\begin{aligned}\lambda_1^{\pm} &= \varepsilon + \frac{k_{21}^2(k_{12}-k_{13}-k_{32}) + k_{21}(k_{11}k_{32}-k_{32}k_{13})}{k_{32}k_{13}}r_1^2 \\ &= \varepsilon + k_{21}\left(\frac{k_{12}}{k_{13}}\left(\frac{k_{21}}{k_{32}}-\frac{k_{21}-k_{11}}{k_{12}}\right)-\frac{k_{21}}{k_{32}}-1\right)r_1^2 \\ &= \varepsilon - \mu_3 k_{21}r_1^2.\end{aligned}$$

This is,

$$\lambda_1^+ = \varepsilon - \mu_3 k_{21}(r_1^+)^2, \qquad \lambda_1^- = \varepsilon - \mu_3 k_{21}(r_1^-)^2.$$

As we did for the eigenvalue λ_2 of the points $Q^{\pm}$, having in mind the definition of $r_1^{\pm}$ (see (4)) it is straightforward to check that

$$\lambda_1^{\pm} = -2\sqrt{\varepsilon_3-\varepsilon}\left(\sqrt{\varepsilon_3-\varepsilon}\pm\sqrt{\varepsilon_3}\right),$$

so then $\lambda_1^+ < 0$ and $\lambda_1^- > 0$. Concerning $\lambda_2^{\pm}$, $\lambda_3^{\pm}$, one has that

$$\lambda_2^+ = \lambda_2^- = -\frac{1}{2}\left(1-\frac{k_{11}}{k_{21}}\right)+\frac{\varepsilon}{2}\sqrt{\Delta},$$
$$\lambda_3^+ = \lambda_3^- = -\frac{1}{2}\left(1-\frac{k_{11}}{k_{21}}\right)-\frac{\varepsilon}{2}\sqrt{\Delta},$$

where Δ has been already defined in (4). Observe that:

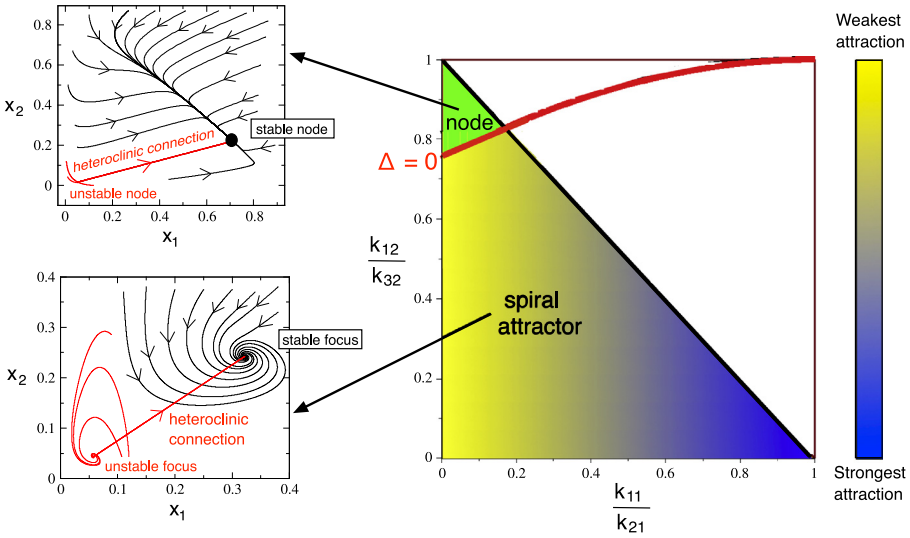

Fig. 15. Biparametric diagram displaying the different dynamics for the three-member hypercycle. The red curve is given by $t = 1 - \frac{1}{4}(1-s)^2$ and corresponds to $\Delta = 0$. Thus, the *yellow–blue* zone represents, in this space of parameters, those values for which $\lambda_2^{\pm,0}$, $\lambda_3^{\pm,0}$ are complex (conjugate). The *green* zone corresponds to those values for which $\lambda_{2,3}^{\pm,0}$ are real (and negative). The phase portraits on the left display the coexistence attractors found in the green (up) and yellow–blue (down) region of the biparametric space (the orbits have been obtained numerically). In red we display the heteroclinic connections, obtained by integrating in negative time starting near the stable fixed point R^+. These heteroclinic trajectories connect the point R^- to the point R^+: (top) saddle–node to stable node; (bottom) unstable node × stable focus to stable node × stable focus. (For interpretation of the references to color in this figure legend, the reader is referred to the web version of this article.)

- If $\Delta \geq 0$ then $\lambda_{2,3}^{\pm}$ are real and since $|\Delta| < 1 - k_{11}/k_{21}$ then $\lambda_{2,3}^{\pm} < 0$. Moreover $|\lambda_3^{\pm}| > |\lambda_2^{\pm}|$.
- If $\Delta < 0$ then $\lambda_{2,3}^{\pm}$ are complex and $\mathrm{Re}\,\lambda_{2,3}^{\pm} = -\frac{1}{2}\left(1 - \frac{k_{11}}{k_{21}}\right) < 0$.

Regarding the point R^0, corresponding to $\varepsilon = \varepsilon_3$, the same expressions obtained for $\lambda_{1,2,3}^{\pm}$ hold, that is

$$\lambda_2^0 = -\frac{1}{2}\left(1 - \frac{k_{11}}{k_{21}}\right) + \frac{\varepsilon_3}{2}\sqrt{\Delta},$$

$$\lambda_3^0 = -\frac{1}{2}\left(1 - \frac{k_{11}}{k_{21}}\right) - \frac{\varepsilon_3}{2}\sqrt{\Delta},$$

and, last but not least, using that $r_1^0 = 1/2\mu_3$, it follows that $\lambda_1^0 = 0$.

One can represent graphically the focus-node transition in the eigenvalues $\lambda_{2,3}^{\pm,0}$. To do it, let us denote $s = k_{11}/k_{21}$ and $t = k_{12}/k_{32}$. From the assumptions $k_{11} < k_{21}$ and $(k_{11}/k_{21}) + (k_{12}/k_{32}) < 1$ it follows that $(s, t) \in (0, 1)$ and satisfy $s + t < 1$. The bifurcation curve $\Delta = 0$ reads $t = 1-(1-s)^2/4$ and separates both behaviors (see Fig. 15).

References

[1] S. Kauffman, The Origins of Order, Press, Oxford University, 1993.
[2] Stanley L. Miller, A production of amino acids under possible primitive earth conditions, Science 117 (3046) (2008) 528–529.
[3] N.H. Horowitz, F.D. Drake, S.L. Miller, L.E. Orgel, C. Sagan, The origins of life, in: P. Handler (Ed.), Biol. Futur. or Man, Oxford University Press, London, 1970.
[4] A. Oparin, Evolution of the concepts of the origin of life, 1924-1974, Orig. Life 7 (2) (1976) 3–8.
[5] Lynn Margulis, Peter Mazur, Elso S. Barghoorn, Harlyn O. Halvorson, Thomas H. Jukes, Isaac R. Kaplan, The viking mission: Implications for life on mars, J. Mol. Evol. 14 (1979) 223–232.
[6] C.R. Woese, A proposal concerning the origin of life on the planet earth, J. Mol. Evol. 13 (1979) 95–101.
[7] J. Oró, A.P. Kimball, Synthesis of purines under possible primitive earth conditions. I. Adenine from hydrogen cyanide, Arch. Biochem. Biophys. 94 (2) (1961) 217–227.
[8] J. Oró, A.P. Kimball, Synthesis of purines under possible primitive earth conditions. II. Purine intermediates from hydrogen cyanide, Arch. Biochem. Biophys. 96 (2) (1962) 293–313.
[9] C.U. Lowe, M.W. Rees, R. Markham, Synthesis of complex organic compounds from simple precursors: Formation of amino-acids, amino-acid polymers, fatty acids, and purines from ammonium cyanide, Nature 199 (1963) 219–222.
[10] P. Eigen, M. Schuster, The Hypercycle. A Principle of Natural Self-organization, Springer-Verlag, 1979.
[11] D. Pörschke, Elementary steps of base recognition and helix-coil transitions in nucleic acids, in: I. Pecht, R. Rigler (Eds.), Chem. Relax. Mol. Biol., Springer-Verlag, 1977, pp. 191–218 (Chapter 24).
[12] U. Niesert, D. Harnasch, C. Bresch, Origin of life between scylla and charybdis, J. Mol. Evol. 17 (1981) 348–353.
[13] Manfred Eigen, Self organization of matter and the evolution of biological macromolecules, Naturwissenschaften 58 (10) (1971) 465–523.
[14] D.A. Usher, A.H. Mchale, Hydrolytic stability of helical RNA: A selective advantage for the, Proc. Natl. Acad. Sci. 73 (4) (1976) 1149–1153.
[15] R. Lohrmann, L.E. Orgel, San Diego, Self-condensation of activated dinucleotides of polynucleotide templates with alternating sequences, J. Mol. Evol. 14 (1979) 243–250.
[16] José-Antonio Daròs, *Eggplant latent viroid*: a friendly experimental system in the family *Avsunviroidae*, Mol. Plant Pathol. 17 (2016) 1170–1177.
[17] Randi M. Jimenez, Julio A. Polanco, Andrej Lupták, Chemistry and biology of self-cleaving ribozymes, Trends Biochem. Sci. 40 (2015) 648–661.
[18] F.H.C. Crick, A speculation on the origin of protein synthesis, Orig. Life 8 (1) (1977) 67.
[19] M.D. Been, E.T. Barford, J.M. Burke, J.V. Price, N.K. Tanner, A.J. Zaug, T.R. Cech, Structures involved in Tetrahymena rRNA self-splicing and RNA enzyme activity, Cold Spring Harb. Symp. Quant. Biol. 52 (1987) 147–157.
[20] T.R. Cech, The chemistry of self-replicating RNA and RNA enzymes, Science 236 (1987) 1532–1539.
[21] Günther Von Kiedrowski, A self-replicating hexadeoxynucleotide, Angew. Chem., Int. Ed. 119 (10) (1986) 932–935.
[22] W.S. Zielinski, L.E. Orgel, Oligomerization of activated derivatives of 3'-amino-3'-deoxyguanosine on poly(C) and poly(dC) templates, Nucleic Acids Res. 13 (24) (1985) 8999–9009.
[23] James Attwater, Aniela Wochner, Philipp Holliger, In-ice evolution of RNA polymerase ribozyme activity, Nature Chem. 5 (12) (2013) 1011–1018.
[24] Nilesh Vaidya, Michael L. Manapat, Irene A. Chen, Ramon Xulvi-Brunet, Eric J. Hayden, Niles Lehman, Spontaneous network formation among cooperative RNA replicators, Nature 491 (2012) 72–77.
[25] Daniel Segré, Dafna Ben-Eli, David W. Deamer, Doron Lancet, The lipid world, Orig. Life Evol. Biosph. 31 (1–2) (2001) 119–145.
[26] D. Segré, D. Ben-Eli, D. Lancet, Compositional genomes: prebiotic information transfer in mutually catalytic noncovalent assemblies, Proc. Natl. Acad. Sci. USA 97 (8) (2000) 4112–4117.
[27] Vera Vasas, Chrisantha Fernando, András Szilágyi, István Zachár, Mauro Santos, Eörs Szathmáry, Primordial evolvability: Impasses and challenges, J. Theoret. Biol. 381 (2015) 29–38.
[28] U. Müller-Herold, What is a Hypercycle? J. Theoret. Biol. 102 (1983) 569–584.
[29] Manfred Eigen, John McCaskill, Peter Schuster, Molecular quasi-species, J. Phys. Chem. 92 (1) (1988) 6881–6891.

[30] Rudolf Hanel, Stuart A. Kauffman, Stefan Thurner, Phase transition in random catalytic networks, Phys. Rev. E 72 (3) (2005) 36117.
[31] Sanjay Jain, Sandeep Krishna, Autocatalytic sets and the growth of complexity in an evolutionary model, Phys. Rev. Lett. 81 (25) (1998) 5684–5687.
[32] S. Jain, S. Krishna, A model for the emergence of cooperation, interdependence, and structure in evolving networks, Proc. Natl. Acad. Sci. USA 98 (2) (2001) 543–547.
[33] P. Boerlijst, M.C. Hogeweg, Spiral wave structure in pre-biotic evolution: Hypercycles stable against parasites, Physica D 48 (1991) 17–28.
[34] Josep Sardanyés, Ricard V. Solé, Spatio-temporal dynamics in simple asymmetric hypercycles under weak parasitic coupling, Physica D 231 (2) (2007) 116–129.
[35] Pan-Jun Kim, Hawoong Jeong, Spatio-temporal dynamics in the origin of genetic information, Physica D 203 (December 2003) (2005) 88–99.
[36] J.M. Smith, E. Szathmáry, The Major Transitions in Evolution, Oxford University Press, 2001.
[37] I. Parsons, M.R. Lee, J.V. Smith, Biochemical evolution II: origin of life in tubular microstructures on weathered feldspar surfaces, Proc. Natl. Acad. Sci. USA 95 (26) (1998) 15173–15176.
[38] Josep Sardanyés, Ricard V. Solé, Delayed transitions in non-linear replicator networks: About ghosts and hypercycles, Chaos Solitons Fractals 31 (2) (2007) 305–315.
[39] István Scheuring, Tamás Czárán, Péter Szabó, György Károlyi, Zoltán Toroczkai, Spatial models of prebiotic evolution: Soup before pizza? Orig. Life Evol. Biosph. 33 (2003) 319–355.
[40] C.S.O. Attolini, Peter F. Stadler, Evolving towards the hypercycle: A spatial model of molecular evolution, Physica D 217 (217) (2006) 134–141.
[41] Josep Sardanyés, Ricard V. Solé, Bifurcations and phase transitions in spatially extended two-member hypercycles, J. Theoret. Biol. 243 (4) (2006) 468–482.
[42] Josep Sardanyés, Error threshold ghosts in a simple hypercycle with error prone self-replication, Chaos Solitons Fractals 35 (2) (2008) 313–319.
[43] Mikael B. Cronhjort, Cluster compartmentalization may provide resistance to parasites for catalytic networks, Physica D 101 (1997) 289–298.
[44] William Harcombe, Novel cooperation experimentally evolved between species, Evolution (NY) 64 (7) (2010) 2166–2172.
[45] Wenying Shou, Sri Ram, Jose M.G. Vilar, Synthetic cooperation in engineered yeast populations, Proc. Natl. Acad. Sci. USA 104 (6) (2007) 1877–1882.